distributed over a region of approximately 11 Mb. The region is centered on our linkage peak and corresponds to the 2-lod drop. The density of markers is greater in the central 3.7-Mb portion of the region, which includes the 1-lod drop, with an average spacing of one marker every 53 kb. We have designated this central region, which is flanked by markers *D5S1474* and *D5S398*, the *STRK1* interval. Three markers, AC027322-5, *D5S2121* and AC008818-1 had different allelic frequencies in affected individuals versus controls with values of $P < 0.01$ (**Table 1**). Correcting for the relatedness of the affected individuals had little impact on the *P* values, but after correcting for the number of markers and alleles tested, none of these *P* values were significant (**Table 1**).

We had previously observed that our linkage peak increased, though not significantly, when we excluded those affected with hemorrhagic stroke. We therefore also tested those affected with ischemic stroke or TIA for association to the markers. In addition, those affected with ischemic stroke and TIA were subclassified according to the TOAST research criteria, and we repeated the association analysis separately for the three TOAST subcategories: cardiogenic, carotid and small vessel occlusive disease. Finally, we tested the combination of those affected with either cardiogenic or carotid stroke, as these categories of stroke are most clearly related to atherosclerosis. The results for each of these association studies are presented in **Supplementary Table 1** online. Three of the markers were significantly associated, one for cardiogenic stroke (AC008818-1), one for carotid stroke (*DG5S397*) and one for the combination of carotid and cardiogenic stroke (AC008818-1), even after correcting for multiple testing (**Table 1**). The marker *DG5S397* is located within *PDE4D*; AC008818-1 is in the 5′ end of *PDE4D* and in the overlapping gene *PART1* (prostate androgen-regulated transcript), whose transcript is on the other strand going in the opposite direction. **Supplementary Fig. 1** online shows the locations of these and other markers relative to the genes in the *STRK1* interval.

PDE4D is an important regulator of intracellular levels of cAMP and is expressed widely. *PART1* encodes a putative protein with unknown function highly expressed in prostate and several tumor cell lines. Physical locations of all genotyped markers and *PDE4D* and *PART1* exons are available in **Supplementary Table 2** online. The association results for the combination of carotid and cardiogenic stroke were particularly notable, with an allele frequency for allele 0 (the CEPH reference allele) of marker AC008818-1 of 35.5% in affected individuals versus 25.5% in controls. The unadjusted *P* value for this marker is 0.0000015; after adjusting for multiple testing of markers, the *P* value is 0.00025 (**Table 1**). This is significant even after adjusting for the several phenotypes studied. The risk of this allele to the other alleles of this marker, assuming the multiplicative model[18,19], was estimated to be 1.60 with a corresponding population attributable risk of 25%. Thus, the strong association signals from our initial microsatellite association studies helped to focus our attention on the *STRK1* interval and, in particular, on the *PDE4D* gene region.

Screening for polymorphisms in *PDE4D*

We next considered whether a functional variant in *PDE4D* might be the cause of our observed microsatellite association. We matched

Table 1 Microsatellite and SNP allelic association

Phenotype	Marker	Allele	*P* value	*P* value[a]	*P* value[b]	RR	# Aff.	% Aff.	# Control	% Control
All affected	AC027322-5	10	0.0010	0.0012	NS	3.34	787	1.9	779	0.6
	D5S2121	−2	0.0027	0.0034	NS	2.19	824	2.7	870	1.3
	AC008818-1	0	0.0045	0.0050	NS	1.25	815	29.9	891	25.5
Cardiogenic	AC008818-1	0	0.000054	0.000077	0.011	1.60	216	35.4	891	25.5
	D5S1990	20	0.00053	0.00088	NS	2.18	223	7.9	879	3.8
	D5S2089	−10	0.0027	0.0040	NS	2.22	219	5.9	813	2.8
Carotid	*DG5S397*	4	0.00024	0.00031	0.045	1.70	124	65.7	577	53.0
	DG5S2056	12	0.00091	0.0019	NS	3.33	80	8.8	464	2.8
	AC008818-1	0	0.0010	0.0014	NS	1.61	125	35.6	891	25.5
Combined cardiogenic	AC008818-1	0	0.0000015	0.0000024	0.00025	1.60	341	35.5	891	25.5
and carotid	AC008833-6	0	0.0026	0.0032	NS	1.35	335	70.3	868	63.8
	DG5S2066	0	0.0032	0.0039	NS	1.74	258	92.3	501	87.2
All affected	SNP32	C	0.00024	0.00027	NS	1.46	400	37.9	475	29.5
	SNP56	T	0.0028	0.0031	NS	1.31	550	71.4	615	65.5
	SNP45	G	0.0065	0.0077	NS	1.33	723	82.4	492	78.0
Cardiogenic	SNP89	A	0.00023	0.00031	NS	2.10	150	90.0	450	81.1
	SNP45	G	0.00041	0.00053	NS	1.77	196	86.2	492	77.9
	SNP91	G	0.00047	0.00059	NS	2.02	151	89.7	451	81.3
Carotid	SNP83	C	0.00043	0.00053	0.045	1.94	76	67.8	349	52.0
	SNP87	T	0.00058	0.00063	NS	1.74	96	62.0	583	48.4
	SNP100	T	0.0010	0.0012	NS	1.79	99	36.4	339	24.2
Combined cardiogenic	SNP45	G	0.000034	0.000044	0.005	1.77	309	86.3	492	78.0
and carotid	SNP41	A	0.000078	0.000096	0.011	1.86	236	86.0	368	76.8
	SNP87	T	0.00019	0.00026	0.031	1.49	263	58.2	583	48.4
	SNP89	A	0.00025	0.00030	0.037	1.85	232	88.8	450	81.1
	SNP56	T	0.00027	0.00034	0.041	1.56	230	74.8	615	65.5

[a]*P* values adjusted for the relatedness of the affected. [b]*P* values adjusted for all the markers tested.

Presented in the table are the three most significant single-marker association results for the disease categories and all signals that survive correction for multiple testing. This is shown both for microsatellites (upper part) and for SNPs (lower part). For the microsatellites, the number reported as an allele is the offset from the smaller of the two alleles of CEPH sample 1347-02 (CEPH genomic repository); thus, allele 0 serves as a (CEPH) reference allele.

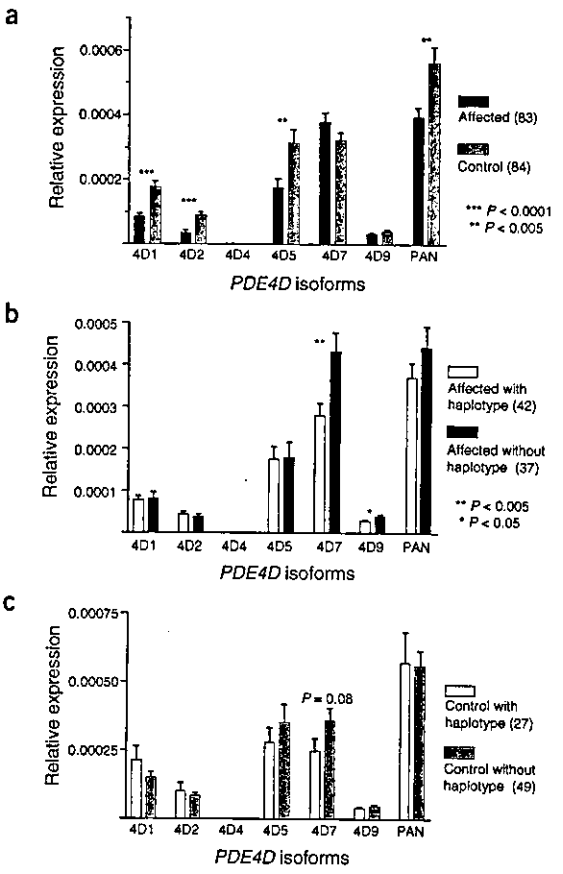

Figure 1 Expression of *PDE4D* isoforms in affected individuals and controls. Expression of *PDE4D* is shown relative to the expression of *GAPD* (as a housekeeping gene). The difference in expression between cases and controls was tested using a two-sample *t*-test on the log-transformed values. Two-sided *P* values are reported. Number of samples is given in parentheses. PAN, total expression of all isoforms. (a) Isoform-specific expression of *PDE4D* mRNA from a randomly selected cohort of affected individuals (red) and controls (blue). (b,c) Corresponding analysis comparing affected individuals (b) or controls (c) with (white bars) and without (colored bars) the at-risk haplotype G0 at the 5′ end of the gene.

public domain expressed-sequence tags and our own RT–PCR and RACE transcripts to our sequence of the *STRK1* interval and defined new alternative *PDE4D* transcripts (**Supplementary Note** online). *PDE4D* contains at least 22 exons over approximately 1.5 Mb overlapping with *PART1*. It encodes eight protein isoforms and has at least seven promoters. All isoforms identified have an identical C-terminal catalytic domain but differ at the N-terminal regulatory domain (**Supplementary Fig. 2** online).

We then attempted to identify mutations by sequencing all known *PDE4D* exons (including the overlapping *PART1* exons) and, on average, 100 bp of their flanking introns in 188 individuals affected with stroke and 94 controls. We identified 46 polymorphisms: 44 single-nucleotide polymorphisms (SNPs) and two intronic deletions. Only two of the polymorphisms, both SNPs, were found within the coding exons of *PDE4D*, consistent with the extraordinary lack of variation that others have reported for all four PDE4 classes[20]. We genotyped the two coding SNPs in additional affected individuals and controls, but they did not show significant association to stroke (**Supplementary Table 3** online). Therefore, if a functional variant conferring risk for stroke exists in *PDE4D*, it may be located in regulatory regions affecting transcription, splicing, message stability or message transport of one or more isoforms or in exons that we have not yet identified.

PDE4D isoform expression

Because we found no functional mutations in the known coding exons of *PDE4D*, we considered other evidence for this gene underlying the association in this region. We studied the expression levels of the various *PDE4D* isoforms, as significant differences between affected individuals and controls could indicate that regulation of *PDE4D* is a key element in stroke susceptibility. We used EBV-transformed B-cell lines from randomly selected affected individuals with ischemic stroke or TIA and from controls. We carried out isoform-specific kinetic RT–PCR analysis to quantify each isoform in 83 individuals with stroke and 84 controls. Most of the affected individuals had ischemic stroke, and 38% had cardiogenic or carotid stroke. We observed that the total *PDE4D* message level, as assessed by amplification across exons present in all isoforms, was significantly lower in affected individuals than in controls ($P = 0.0021$). This difference was due primarily to lower expression of the *PDE4D1*, *PDE4D2* and *PDE4D5* isoforms (**Fig. 1a**). This significant disregulation of the expression of multiple *PDE4D* isoforms encouraged us to continue investigating the association of *PDE4D* with stroke.

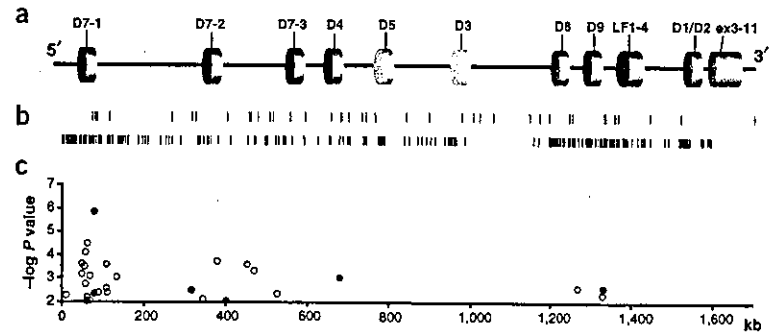

Figure 2 Single-marker allelic association within *PDE4D*. The same horizontal scales are used for **a**, **b** and **c**. (a) *PDE4D* gene structure. Exons are shown as colored cylinders and exon names are indicated above the line. (b) Microsatellite and SNP distribution in the gene. Red vertical bars indicate microsatellites and blue vertical bars SNPs. (c) Single-marker allelic association across *PDE4D* for both microsatellites (filled circles) and SNPs (open circles). The plot shows negative log *P* value versus the physical location in kilobases. Results with *P* values of 0.01 or less are shown for all stroke cases (black) and for the combination of cardiogenic and carotid cases (red).

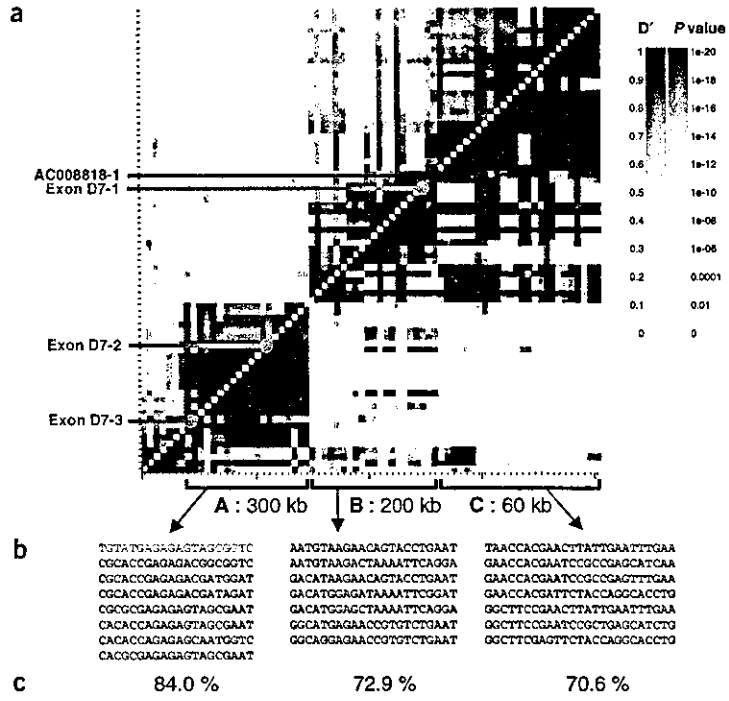

Figure 3 LD and haplotypes at the 5′ end of *PDE4D*. (a) Pairwise linkage disequilibrium between SNPs in a 600-kb region in the 5′ end of *PDE4D*. The markers are plotted equidistantly. Two measures of LD are shown: *D′* in the upper left triangle and *P* values in the lower right triangle. This region can be divided into three blocks of strong LD, each with limited haplotype diversity: block A, block B and block C. Colored lines indicate the position of the three exons, D7-1, D7-2 and D7-3, and the microsatellite marker, AC008818-1. (b) All common haplotypes identified in each of the three blocks. The haplotypes in each block showing strongest association with stroke are colored green, blue and red. Association results for all haplotypes are presented in **Supplementary Table 6** online. (c) The percentage of chromosomes in each block that match one of the common haplotypes.

SNPs: marker association and linkage disequilibrium

We next searched for SNPs in the intronic and flanking regions of *PDE4D* in the public National Center for Biotechnology Information SNP database or by sequencing selected intronic and flanking regions in the gene in at least 94 affected individuals and 94 controls. We initially identified 637 SNPS. Many of these SNPs were completely correlated so we removed several redundant SNPs from further genotyping. Some SNPs with very low minor allele frequencies were also ignored. This resulted in a set of 260 SNPs that were then genotyped in the entire affected and control cohorts. We determined the exonic structure of *PDE4D* (**Fig. 2a**) relative to the location of SNPs and microsatellite markers (**Fig. 2b**) and carried out single-marker SNP and microsatellite association tests for all markers (**Fig. 2c**).

Most markers with significant associations were located at the 5′ end of the gene. One SNP (SNP83) associated with carotid stroke and five of the SNPs (SNP45, SNP41, SNP87, SNP89 and SNP56) associated with the combined cardiogenic and carotid stroke were significant even after adjusting for all the SNPs tested (**Table 1**). Three of these significant SNPs flank exon D7-1; the other three are in a 100-kb region containing exon D7-2 (for physical positions see **Supplementary Table 2** online). Some additional results for the single-point SNP associations are supplied in **Supplementary Table 4** online.

The two most significant SNPs, SNP45 and SNP41, are within 6 kb of the microsatellite marker AC008818-1, and the at-risk alleles of all three genetic markers are in strong linkage disequilibrium (LD) with $D' > 0.9$ and *P* value nearly zero (**Supplementary Table 5** online). The square of the correlation (R^2) is very high between the two SNPs (~0.93) but is substantially lower (~0.08) between each SNP and the at-risk allele of the microsatellite. This is because the frequency of the at-risk alleles of the two SNPs are similar and much higher than that of the at-risk allele of the microsatellite. We determined the LD block structure around the 5′ end of *PDE4D* (**Fig. 3a**). We delineated three blocks, A, B and C, encompassing the first three exons of *PDE4D* and its immediate upstream region. Exons D7-3 and D7-2 are both in block A, and D7-1 (the first exon) is in block B, close to its border with block C. Given this block structure, we were prepared to investigate haplotypes associated with susceptibility to stroke in this region.

Haplotype association

We first considered haplotypes based on the most significantly associated SNPs and microsatellite, SNP45, SNP41 and AC008818-1, all in block B separated by only 6 kb. As expected given the high degree of correlation between SNP45 and SNP41, we found that it was sufficient to consider only the two marker haplotypes consisting of the microsatellite and SNP45, the SNP with the higher genotype yield. The results of this association study for the combination of carotid and cardiogenic stroke are shown in **Figure 4a**. The letter X designates the joint set of alleles, excluding the at-risk allele 0, of microsatellite AC008818-1. GX is therefore the composite of all haplotypes including the G nucleotide of SNP45 except for the G0 haplotype. For our samples, the A0 haplotype does not exist. This suggests that allele 0 originated in a haplotype background with allele G of SNP45 and since then, no recombination has occurred between those two markers for chromosomes that carried allele 0.

Haplotypes AX, G0 and GX carry significantly different risks for the combined carotid and cardiogenic stroke phenotype. We consider haplotype GX to be the wild type as it is the most common (53.4% in controls) and also because it carries an intermediate level risk not too different from the population risk. Haplotype G0 carries higher risk and haplotype AX is protective, with risks of 1.46 and 0.70 relative to the wild type, respectively. The risk associated with haplotype G0 is 2.07 times that of the protective haplotype AX. Each of the three pairwise comparisons was highly significant, with *P* values ranging from 0.006 to 7.2×10^{-8}. Both haplotypes AX and GX are composite haplotypes, but the AX haplotype can be simply summarized by the allele A of SNP45, as the haplotype A0 does not exist. Similarly, the G0 haplotype is completely determined by the 0 allele of AC008818-1.

Figure 4a also shows the information content (Info) of each test. The difference between Info and 1 is a measure of the information that is lost owing to the uncertainty with phase and missing geno-

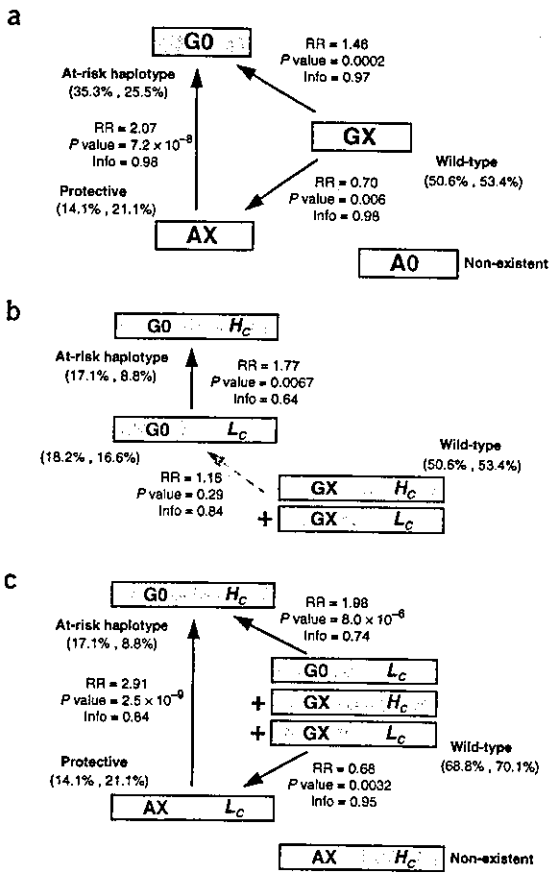

Figure 4 Haplotype association for carotid and cardiogenic stroke combined. Estimated haplotype frequencies for affected individuals and controls, in that order, are given in parentheses. (**a**) Comparisons of groups of haplotypes constructed from SNP45 and AC008818-1, two markers separated by 6 kb. X is a composite allele denoting all alleles of AC008818-1 except allele 0. Apart from haplotype A0, which is not found in our samples, other haplotypes can be grouped into three groups with distinct risks. Each arrow corresponds to a comparison between two groups, and RR is the estimated risk of the group the arrow is pointing at relative to the other group. (**b**) Intermediate results when the investigation is extended from SNP45 and AC008818-1, which are both in LD block B, to include 25 SNPs in LD block C. H_C is the at-risk haplotype, identified in **Figure 3** (colored in red), and L_C is a composite haplotype denoting all haplotypes of the 25 SNPs except H_C. Together with AC008818-1 and SNP45, the haplotypes here span 64 kb. Haplotype G0 in **a** is split into extended haplotypes G0H_C and G0L_C. G0H_C has significantly higher risk than G0L_C, and the risk of G0L_C is not distinguishable from that of the wild-type GX. (**c**) A refinement of the groupings in **a**. G0L_C is moved from the at-risk group to the wild-type group. The extended haplotype AXH_C does not exist, indicating that blocks B and C are in LD.

types (see **Supplementary Note** online for details). Info is very close to 1 for each of the three pairwise comparisons (**Fig. 4a**). This is a result of SNP45 and AC008818-1 being in very strong LD. Tests presented in **Figure 4b,c**, which involve longer haplotypes, have lower information content.

We next identified and estimated the risks for the common SNP haplotypes in each block, considering only those SNPs with minor allele frequency greater than 20%. Block A (300 kb) contained 19 such SNPs, block B (200 kb) 22 SNPs and block C (60 kb) 25 SNPs. We identified all haplotypes in each block with an estimated frequency in the population of 2% or greater. In each block there were fewer than ten such haplotypes, and they accounted for approximately 80% of the total haplotype frequency for that block. A brief schematic of the identified haplotypes is given in **Figure 3b**, and the risks and frequencies of these haplotypes are available in **Supplementary Table 6** online. In block A, no common haplotype has greater risk than SNP87 alone. The strongest signals were for haplotypes in block B and C. Each block contained a haplotype significantly associated with the combination of carotid and cardiogenic stroke and having relative risk around 1.5. The common at-risk haplotype in block B is the SNP background of the G0 haplotype previously identified.

Although there were no significant single-marker associations in block C, we observed a common haplotype with 15.4% frequency in controls, which we designate haplotype H_C. All haplotypes defined by the 25 SNPs in block C that are not H_C are jointly denoted by the composite haplotype L_C. We investigated the contribution of H_C in conjunction with the SNP45 and AC008818-1 haplotypes. AX and H_C do not exist together on the same chromosome (**Fig. 4c**), at least in these samples. Thus, blocks B and C are far from being independent, and the extended composite haplotype AXL_C is the same as AX. The haplotype G0 can be split into the two extended haplotypes G0H_C and the composite G0L_C, which have significantly different risks ($P = 0.0067$; **Fig. 4b**). Moreover, the high risk associated with G0 is totally accounted for by G0H_C, as G0L_C has risk that is not significantly different from GX (GX = GXH_C + GXL_C; **Fig. 4b**). This observation allowed us to refine our initial haplotype groupings (**Fig. 3a,c**). The extended at-risk haplotype G0H_C (8.8% in controls) and protective composite haplotype AXL_C (21.1% in controls) have relative risks of 1.98 and 0.68, respectively, relative to the wild type (70.1% in controls). Based on these risk estimates, if everybody's risk corresponded to that of a homozygous carrier of the protective variant, the number of cases would be reduced by 55%, which can be interpreted as the population-attributed risk of the at-risk haplotype and the wild-type combined.

The at-risk haplotype G0H_C spans a region of about 64 kb. It is possible that the greater risk is due to multiple polymorphisms over that region, but the results are also consistent with this region harboring a relatively recent mutation (as yet unidentified) that occurred in that haplotype background, with no recombination occurring since then for chromosomes carrying the mutation. By contrast, the protective composite haplotype AXL_C can be simply represented by allele A of SNP45. Hence, it is possible that allele A of SNP45 is the functional protective variant, although it is possible that the functional variant is simply in strong LD with allele A of SNP45 and has not yet been identified. Statistically, the effects of SNP45 and SNP41 are indistinguishable from each other.

We reanalyzed the *PDE4D* isoform expression data for those with haplotype G0 versus those without that haplotype both in affected individuals and in controls. For the samples in the expression study, the frequency of the G0 haplotype was 29.4% in affected individuals and 25.2% in controls. Those affected with the haplotype had significantly lower expression of the *PDE4D7* and *PDE4D9* isoforms (**Fig. 1b**). Other isoforms of *PED4D* did not significantly correlate with the disease-associated haplotype. The correlation of *PDE4D7* with the haplotype was also present in controls but was only marginally significant (**Fig. 1c**).

DISCUSSION

Our results indicate that variations in *PDE4D* are associated with ischemic stroke. The direct involvement of *PDE4D* is strongly supported by linkage in conjunction with association and expression analysis. We first identified the association using microsatellite markers and then supplemented the microsatellite data with a denser set of SNPs. The strongest association was with the two ischemic subtypes, carotid and cardiogenic stroke. We examined whether the disease-associated alleles and haplotype were related to specific stroke risk factors, such as hypertension, hypercholesterolemia, diabetes, peripheral artery occlusive disease and coronary artery disease in addition to early onset of stroke and sex (**Supplementary Table 7** online). We observed a marginally significant association to hypercholesterolemia, but the contribution of *PDE4D* to stroke is clearly not strongly correlated with any of these known risk factors.

For the combined cardiogenic and carotid subtype of stroke, it is notable that haplotypes covering the first exon of *PDE4D* can be classified into three groups with clearly distinct risks. Relative to the protective group, the general population-attributed risk of the at-risk and wild-type groups combined is estimated to be 55%. Approximately 16% of the general population carries one copy of the at-risk haplotype (**Fig. 4c**). They have about 1.8 times higher risk than the general population for cardiogenic or carotid stroke. Approximately 0.8% of the population are homozygous with respect to the at-risk haplotype and, assuming the multiplicative model, their risk is estimated to be about 3.8 times than that of the general population. We have not yet identified the functional variants that are responsible for the observed effects of these haplotype groups. And, because these haplotype groups do not fully explain the linkage signal we observe in the region for all affected individuals, we certainly could not rule out, and indeed expect, that there are other variants or haplotypes in *PDE4D* not directly related to those we have identified that confer risk to stroke. These are probably rare but could have very high penetrance. We also cannot rule out the possibility that some other genes in the linkage region independent of, or in conjunction with, *PDE4D* confer susceptibility to stroke.

By alternative splicing and using different promoters, *PDE4D* generates at least eight different isoforms that yield functional proteins, differing from each other at their N-terminal regions. We identified four new exons encoding the N-termini of two new isoforms, *PDE4D7* and *PDE4D9*. The disease-associated haplotype extends over the 5′ exon unique to the new *PDE4D7* variant and the presumed promoter region of this isoform, suggesting that the functional variation may be involved in transcriptional regulation. This hypothesis is also supported by our *PDE4D* expression analysis showing that there is significant correlation between the disease-associated haplotype and the level of *PDE4D7* message.

The strongest association found for this *PDE4D* haplotype was to the two main subtypes of ischemic stroke, cardiogenic and carotid stroke, suggesting a role for this gene in the vascular biology of atherosclerosis. Although there are multiple etiologies for ischemic stroke, atherosclerosis is the most important and is the primary pathological process for cardiogenic and carotid stroke. First, it is the main cause of stenotic and occlusive lesions of the internal and common carotids that lead to carotid strokes. Second, cardiac thrombi, which shed emboli to the brain, most commonly occur on the background of coronary artery disease (such as after acute myocardial infarction or ischemic cardiomyopathy) or as a result of atrial fibrillation due to poor compliance of ischemic ventricles (diastolic dysfunction/stiffening). Although atrial fibrillation may occur on the background of other diseases, such as valvular disease, hyperthyroidism and hypertension, in the age group that tends to suffer from stroke, ischemic heart disease is one of the main causes. Ischemic stroke resulting from occlusion of small penetrating arteries in the brain (small vessel occlusive disease) is generally thought to result from endothelial proliferation, as atherosclerosis only occurs in larger arteries. *PDE4D* does not show association to small vessel stroke, consistent with its role in atherosclerosis.

What biological role does *PDE4D* have in predisposition to stroke, in particular, and to the underlying atherosclerosis? PDE4D selectively degrades second messenger cAMP[20], which has a central role in signal transduction and regulation of physiological responses. It is expressed in most cell types important to the pathogenesis of atherosclerosis, including vascular smooth muscle cells, endothelial cells, T-lymphocytes, macrophages[21–25] and monocytes (data not shown). Cyclic AMP is a key signaling molecule in these cells[26–28]. In vascular smooth muscle cells, low cAMP levels lead to an increase in proliferation and migration that is mediated, at least in part, by PDE4 (refs. 26,29,30). Animal models have also shown that elevation of cAMP reduces neointimal lesion formation and inhibits proliferation of smooth muscle cells after arterial injury[31,32]. In monocytes and T-lymphocytes, accumulation of cAMP is generally associated with inhibition of immune functions, such as proliferation and cytokine secretion[33].

One could postulate that the regulation of cAMP through absolute or relative expression of one or more *PDE4D* isoforms may differ in individuals susceptible to stroke; some may have greater PDE4D activity and, consequently, lower cAMP levels in any of the above cell types, leading to development of the atherosclerotic plaque or to its instability. Contrary to what one might expect, however, we observed lower expression of some of the *PDE4D* isoforms in EBV cell lines from affected individuals. These isoforms are upregulated by cAMP[22,34,35], suggesting disregulation at the level of cAMP in affected individuals. It is therefore possible that greater activity of one or few splice variants alters the effective PDE4D enzymatic activity of the cell, decreasing the cAMP levels and thus altering the expression of cAMP-regulated isoforms as observed in our expression study. This relative expression of *PDE4D* isoforms may determine the compartmental localization of *PDE4D* isoforms and thus the corresponding gradients of intracellular cAMP that have been recently observed[20].

In summary, we present association analyses (single-marker and haplotype analyses) that support the idea that *PDE4D* confers risk of ischemic stroke. Furthermore, we observed significant disregulation of multiple *PDE4D* isoforms in affected individuals. We propose that this gene is involved in the pathogenesis of stroke through atherosclerosis. *PDE4D* is expressed in cell types important in atherosclerosis and regulates a second messenger that has a central role in processes important in the pathogenesis of atherosclerosis. Perhaps inhibition of *PDE4D* in general, or of one or more isoforms specifically, by a small-molecule drug might decrease the risk of stroke in those who are predisposed by genotype at *PDE4D*.

METHODS

Subjects. We recruited individuals with stroke and carried out phenotypic subclassification as previously described[17]. The study was approved by the Data Protection Commission of Iceland and the National Bioethics Committee of Iceland. We obtained informed consent from all affected individuals and their relatives whose DNA samples were used in the analyses. All personal identifiers associated with medical information and blood samples were encrypted with a third party encryption system by the Data Protection Commission[36]. The phenotypes of participating affected individuals were redetermined by neurologists examining the clinical and radiological records, and those affected with ischemic stroke or TIA were subcategorized according to the TOAST research criteria[4]. We used a cutoff of 70% stenosis as the criterion for carotid stroke.

Identification of DNA polymorphisms. We identified new polymorphic repeats (dinucleotide or trinucleotide repeats) with the Sputnik program. We subtracted the smaller allele of CEPH sample 1347-02 (CEPH genomics repository) from the alleles of the microsatellites and used it as a reference. We detected SNPs by sequencing exonic and intronic regions from affected individuals and controls by PCR. We also detected public polymorphisms by BLAST search of the US National Center for Biotechnology Information's SNP database. We genotyped SNPs using a method for detecting SNPs with fluorescent polarization template-directed dye-terminator incorporation (SNP-FP-TDI assay; ref. 37).

Statistical analysis. For single-marker association studies, we used Fisher's exact test to calculate two-sided *P* values for each individual allele. All *P* values are unadjusted for multiple comparisons unless specifically indicated. We present allelic rather than carrier frequencies for microsatellites, SNPs and haplotypes. To minimize any bias due to the relatedness of the affected individuals who were recruited as families for the linkage analysis, we eliminated first- and second-degree relatives from the list of affected individuals. We also repeated the test for association, correcting for any remaining relatedness among the affected individuals by extending a variance adjustment procedure described previously[38] for sibships to apply to general familial relationships, and present both adjusted and unadjusted *P* values for comparison. The differences are generally very small, as expected. To assess the significance of single-marker association corrected for multiple testing, we carried out a randomization test using the same genotype data. We randomized the cohorts of affected individuals and controls and redid the association analysis. This procedure was repeated up to 500,000 times, and the *P* value we present is the fraction of replications that produced a *P* value for some marker allele that is lower than or equal to the *P* value we observed using the original affected and control cohorts.

For both single-marker and haplotype analyses, we calculated relative risk (RR) and population attributable risk assuming a multiplicative model (haplotype relative risk model; refs. 18,19) in which the risks of the two alleles or haplotypes a person carries multiply. For example, if RR is the risk of allele A relative to allele a, then the risk of an AA homozygote will be RR times that of an Aa heterozygote and RR^2 times that of an aa homozygote. The multiplicative model simplifies analysis and computations because haplotypes are independent, meaning they are in Hardy-Weinberg equilibrium in the affected population as well as in the control population. As a consequence, haplotype counts of the affected individuals and controls each have multinomial distributions, but with different haplotype frequencies under the alternative hypothesis. Specifically, for two haplotypes h_i and h_j, $\text{risk}(h_i)/\text{risk}(h_j) = (f_i/p_i)/(f_j/p_j)$, where f and p denote frequencies in the affected population and in the control population, respectively. Although there is some power loss if the true model is not multiplicative, the loss tends to be mild except in extreme cases. Most importantly, *P* values are always valid because they are computed with respect to the null hypothesis.

In general, haplotype frequencies are estimated by maximum likelihood and tests of differences between affected individuals and controls are carried out using a generalized likelihood ratio test[39]. We used our haplotype analysis program, called NEMO (which stands for 'nested models'; see **Supplementary Note** online for more details), to calculate all the haplotype results presented. To handle uncertainties with phase and missing genotypes, we did not use the common two-step approach to association tests, in which haplotype counts are first estimated, possibly with the use of the EM algorithm[40], and tests are then carried out, treating the estimated counts as though they are true counts. This method can be problematic and may require randomization to properly evaluate statistical significance. Instead, with NEMO, maximum likelihood estimates, likelihood ratios and *P* values are computed with the aid of the EM algorithm directly for the observed data; hence, loss of information due to uncertainty with phase and missing genotypes is automatically captured by the likelihood ratios. Even so, how much information is retained or lost may be of interest; **Supplementary Note** online describes such a measure that is natural under the likelihood framework.

For a fixed set of markers, the simplest tests we did (with results presented in **Supplementary Table 6** online) compare one selected haplotype against all the others. Call the selected haplotype h_1 and the others be $h_2, \ldots h_k$. Let $p_1, \ldots p_k$ denote the population frequencies of the haplotypes in the controls, and let $f_1, \ldots f_k$ denote the population frequencies of the haplotypes in the affected individuals. Under the null hypothesis, $f_i = p_i$ for all i. The alternative model we use for the test assumes $h_2, \ldots h_k$ to have the same risk but h_1 has a different risk. This implies that p_1 can be different from f_1, but $f_i/(f_2 + \ldots + f_k) = p_i/(p_2 + \ldots + p_k) = \beta_i$ for $i = 2, \ldots k$. Denoting f_1/p_1 with r, and noting that $\beta_2 + \ldots + \beta_k = 1$, the test statistic based on generalized likelihood ratios is

$$\Lambda = 2\left[l(\hat{r}, \hat{p}_1, \hat{\beta}_2, \ldots, \hat{\beta}_{k-1}) - l(1, \tilde{p}_1, \tilde{\beta}_2, \ldots, \tilde{\beta}_{k-1})\right]$$

where l denotes $\log_e$ likelihood and ˜ and ^ denote maximum likelihood estimates under the null hypothesis and alternative hypothesis, respectively. Λ has asymptotically a χ^2 distribution with 1 degree of freedom under the null hypothesis, and it was used to compute *P* values presented in **Supplementary Table 6** online. The tests presented in **Figure 4** have slightly more complicated null and alternative hypotheses. For the results in **Figure 4a**, let h_1 be G0, h_2 be GX and h_3 be AX. When comparing G0 with GX (the test that gives estimated $RR = 1.46$ and $P = 0.0002$), the null hypothesis assumes G0 and GX have the same risk but AX has a different risk. The alternative hypothesis allows all three haplotype groups to have different risks. This implies that, under the null hypothesis, there is a constraint that $f_1/p_1 = f_2/p_2$, or $w = (f_1/p_1)/(f_2/p_2) = 1$. The test statistic based on generalized likelihood ratios is

$$\Lambda = 2\left[l(\hat{p}_1, \hat{f}_1, \hat{p}_2, \hat{w}) - l(\tilde{p}_1, \tilde{f}_1, \tilde{p}_1, 1)\right]$$

which again has asymptotically a χ^2 distribution with 1 degree of freedom under the null hypothesis. There is actually an extra complication to the test when h_2 and h_3 are composite haplotypes. That is handled in a natural manner under the nested models framework with details given in **Supplementary Note** online. Other tests presented in **Figure 4** were similarly carried out.

We calculated LD between pairs of SNPs using the standard definition of D' (ref. 41) and R^2 (ref. 42). Using NEMO, frequencies of the two marker allele combinations are estimated by maximum likelihood, and deviation from linkage equilibrium is evaluated by a likelihood ratio test. We extended the definitions of D' and R^2 to include microsatellites by averaging over the values for all possible allele combinations the two markers weighted by the marginal allele probabilities. When plotting all marker combinations to elucidate the LD structure in a particular region, we plotted D' in the upper left corner and the *P* value in the lower right corner. In the LD plots we present, the markers are plotted equidistantly rather than according to their physical positions.

Enquiries regarding information and accessibility of the haplotype analysis program NEMO should be addressed to A.K. (augustine.kong@decode.is) or D.G. (daniel.gudbjartsson@decode.is).

Expression analysis using quantitative reverse transcriptase PCR. We isolated total RNA from EBV-transformed B-cell cultures according to the manual using the TRIZOL reagent provided by GibcoBRL. We used the RNeasy mini Qiagen kit with on-column DNA digestion to clean RNA. We assessed the quality and quantity of RNA using 2100 Agilent Bioanalyser. We prepared cDNA from total RNA using random hexamers with TaqMan Reverse Transcription Reagents kit from Applied Biosystems (N808-0234). We used Primer Express 2.0 and Oligo 6 software to make cDNA-specific primers and probes for *PDE4D* and *PDE4D* isoforms. We obtained *GAPD* 'Assay-On-Demand' from Applied Biosystems and used it as a housekeeping gene. We tested PDE assays and optimized them for 384-well high-throughput expression analysis on ABI 7900 Instrument. We used a final concentration of 200 nM probes, 900 nM primers and 2 ng μl^{-1} cDNA in a 10-µl reaction volume. We processed each plate twice and calculated an average for each sample. We used the ABI7900 instrument to calculate CT (Threshold Cycle) values. We calculated quantity estimates using the formula $2^{-\Delta CT}$ where ΔCT represents the difference in CT values for target and housekeeping assays. We eliminated from our analyses any samples whose duplicates differed by more than 1 ΔCT.

URLs. The American Heart Association can be found at http://www.americanheart.org/. The Sputnik program can be found at http://espressosoftware.com/pages/sputnik.jsp. The US National Center for Biotechnology Information's SNP database is found at http://www.ncbi.nlm.nih.gov/SNP/index.html.

GenBank accession numbers. *PDE4D7*, AY245866; *PDE4D9*, AY245867.

Note: Supplementary information is available on the Nature Genetics website.

ACKNOWLEDGMENTS

We thank the affected individuals and their families whose contribution made this study possible and the nurses at the Icelandic Heart Association, staff at the deCODE core facilities and V. Brophy and S. Cheng for their valuable contribution to this work. Enquiries regarding information and accessibility of the haplotype analysis program NEMO should be addressed to A.K. (augustine.kong@decode.is) or D.G. (daniel.gudbjartsson@decode.is).

COMPETING INTERESTS STATEMENT

The authors declare competing financial interests (see the *Nature Genetics* website for details).

Received 1 July; accepted 27 August 2003
Published online at http://www.nature.com/naturegenetics/

1. Sacco, R.L. *et al.* American Heart Association Prevention Conference. IV. Prevention and Rehabilitation of Stroke. Risk factors. *Stroke* **28**, 1507–1517 (1997).
2. Bonita, R. Epidemiology of stroke. *Lancet* **339**, 342–344 (1992).
3. Caplan, L.R. *Caplan's Stroke: A Clinical Approach.* (Butterworth-Heinemann, Boston, 2000).
4. Adams, H.P.Jr. *et al.* Classification of subtype of acute ischemic stroke. Definitions for use in a multicenter clinical trial. TOAST. Trial of Org 10172 in Acute Stroke Treatment. *Stroke* **24**, 35–41 (1993).
5. Fisher, C.M. Lacunar strokes and infarcts: a review. *Neurology* **32**, 871–876 (1982).
6. Alberts, M.J. *Genetics of Cerebrovascular Disease* (Futura, New York, 1999).
7. Hassan, A. & Markus, H.S. Genetics and ischaemic stroke. *Brain* **123**, 1784–1812 (2000).
8. Leys, D. *et al.* Stroke prevention: management of modifiable vascular risk factors. *J. Neurol.* **249**, 507–517 (2002).
9. Brass, L.M. & Alberts, M.J. The genetics of cerebrovascular disease. *Baillieres Clin. Neurol.* **4**, 221–245 (1995).
10. Tournier-Lasserve, E. *et al.* Cerebral autosomal dominant arteriopathy with subcortical infarcts and leukoencephalopathy maps to chromosome 19q12. *Nat. Genet.* **3**, 256–259 (1993).
11. Joutel, A. *et al. Notch3* mutations in CADASIL, a hereditary adult-onset condition causing stroke and dementia. *Nature* **383**, 707–710 (1996).
12. Palsdottir, A. *et al.* Mutation in cystatin C gene causes hereditary brain haemorrhage. *Lancet* **2**, 603–604 (1988).
13. Levy, E. *et al.* Mutation of the Alzheimer's disease amyloid gene in hereditary cerebral hemorrhage, Dutch type. *Science* **248**, 1124–1126 (1990).
14. Gunel, M., Awad, I.A., Anson, J. & Lifton, R.P. Mapping a gene causing cerebral cavernous malformation to 7q11.2–q21. *Proc. Natl. Acad. Sci. USA* **92**, 6620–6624 (1995).
15. Laberge-le Couteulx, S. *et al.* Truncating mutations in *CCM1*, encoding KRIT1, cause hereditary cavernous angiomas. *Nat. Genet.* **23**, 189–193 (1999).
16. Sahoo, T. *et al.* Mutations in the gene encoding KRIT1, a Krev-1/rap1a binding protein, cause cerebral cavernous malformations (CCM1). *Hum. Mol. Genet.* **8**, 2325–2333 (1999).
17. Gretarsdottir, S. *et al.* Localization of a susceptibility gene for common forms of stroke to 5q12. *Am. J. Hum. Genet.* **70**, 593–603 (2002).
18. Terwilliger, J.D. & Ott, J. A haplotype-based 'haplotype relative risk' approach to detecting allelic associations. *Hum. Hered.* **42**, 337–346 (1992).
19. Falk, C.T. & Rubinstein, P. Haplotype relative risks: an easy reliable way to construct a proper control sample for risk calculations. *Ann. Hum. Genet.* **51** (Pt 3), 227–233 (1987).
20. Houslay, M.D. & Adams, D.R. PDE4 cAMP phosphodiesterases: modular enzymes that orchestrate signalling cross-talk, desensitization and compartmentalization. *Biochem. J.* **370**, 1–18 (2003).
21. Liu, H. & Maurice, D.H. Phosphorylation-mediated activation and translocation of the cyclic AMP- specific phosphodiesterase PDE4D3 by cyclic AMP-dependent protein kinase and mitogen-activated protein kinases. A potential mechanism allowing for the coordinated regulation of PDE4D activity and targeting. *J. Biol. Chem.* **274**, 10557–10565 (1999).
22. Liu, H. *et al.* Expression of phosphodiesterase 4D (PDE4D) is regulated by both the cyclic AMP-dependent protein kinase and mitogen-activated protein kinase signaling pathways. A potential mechanism allowing for the coordinated regulation of PDE4D activity and expression in cells. *J. Biol. Chem.* **275**, 26615–26624 (2000).
23. Baillie, G., MacKenzie, S.J. & Houslay, M.D. Phorbol 12-myristate 13-acetate triggers the protein kinase A-mediated phosphorylation and activation of the PDE4D5 cAMP phosphodiesterase in human aortic smooth muscle cells through a route involving extracellular signal regulated kinase (ERK). *Mol. Pharmacol.* **60**, 1100–1111 (2001).
24. Jin, S.L. & Conti, M. Induction of the cyclic nucleotide phosphodiesterase PDE4B is essential for LPS-activated TNF-α responses. *Proc. Natl. Acad. Sci. USA* **99**, 7628–7633 (2002).
25. Landells, L.J. *et al.* Identification and quantification of phosphodiesterase 4 subtypes in CD4 and CD8 lymphocytes from healthy and asthmatic subjects. *Br. J. Pharmacol.* **133**, 722–729 (2001).
26. Fukumoto, S. *et al.* Distinct role of cAMP and cGMP in the cell cycle control of vascular smooth muscle cells: cGMP delays cell cycle transition through suppression of cyclin D1 and cyclin-dependent kinase 4 activation. *Circ. Res.* **85**, 985–991 (1999).
27. Ogawa, S. *et al.* Hypoxia-induced increased permeability of endothelial monolayers occurs through lowering of cellular cAMP levels. *Am. J. Physiol.* **262**, C546–C554 (1992).
28. Stelzner, T.J., Weil, J.V. & O'Brien, R.F. Role of cyclic adenosine monophosphate in the induction of endothelial barrier properties. *J. Cell Physiol.* **139**, 157–166 (1989).
29. Pan, X., Arauz, E., Krzanowski, J.J., Fitzpatrick, D.F. & Polson, J.B. Synergistic interactions between selective pharmacological inhibitors of phosphodiesterase isozyme families PDE III and PDE IV to attenuate proliferation of rat vascular smooth muscle cells. *Biochem. Pharmacol.* **48**, 827–835 (1994).
30. Palmer, D., Tsoi, K. & Maurice, D.H. Synergistic inhibition of vascular smooth muscle cell migration by phosphodiesterase 3 and phosphodiesterase 4 inhibitors. *Circ. Res.* **82**, 852–861 (1998).
31. Indolfi, C. *et al.* Activation of cAMP-PKA signaling *in vivo* inhibits smooth muscle cell proliferation induced by vascular injury. *Nat. Med.* **3**, 775–779 (1997).
32. Indolfi, C. *et al.* 8-chloro-cAMP inhibits smooth muscle cell proliferation *in vitro* and neointima formation induced by balloon injury *in vivo*. *J. Am. Coll. Cardiol.* **36**, 288–293 (2000).
33. Tilley, S.L., Coffman, T.M. & Koller, B.H. Mixed messages: modulation of inflammation and immune responses by prostaglandins and thromboxanes. *J. Clin. Invest.* **108**, 15–23 (2001).
34. Vicini, E. & Conti, M. Characterization of an intronic promoter of a cyclic adenosine 3',5'-monophosphate (cAMP)-specific phosphodiesterase gene that confers hormone and cAMP inducibility. *Mol. Endocrinol.* **11**, 839–850 (1997).
35. Le Jeune, I.R., Shepherd, M., Van Heeke, G., Houslay, M.D. & Hall, I.P. Cyclic AMP-dependent transcriptional up-regulation of phosphodiesterase 4D5 in human airway smooth muscle cells. Identification and characterization of a novel PDE4D5 promoter. *J. Biol. Chem.* **277**, 35980–35989 (2002).
36. Gulcher, J.R., Kristjansson, K., Gudbjartsson, H. & Stefansson, K. Protection of privacy by third-party encryption in genetic research in Iceland. *Eur. J. Hum. Genet.* **8**, 739–742 (2000).
37. Chen, X., Zehnbauer, B., Gnirke, A. & Kwok, P.Y. Fluorescence energy transfer detection as a homogeneous DNA diagnostic method. *Proc. Natl. Acad. Sci. USA* **94**, 10756–10761 (1997).
38. Risch, N. & Teng, J. The relative power of family-based and case-control designs for linkage disequilibrium studies of complex human diseases I. DNA pooling. *Genome Res.* **8**, 1273–1288 (1998).
39. Rice, J.A. Generalized likelihood ratio tests. In *Mathematical Statistics and Data Analysis* 308–310 (International Thomson Publishing, Belmont, California, 1995).
40. Dempster, A.P., Laird, N.M. & Rubin, D.B. Maximum likelihood estimation from incomplete data via the EM algorithm (with discussion). *J. R. Stat. Soc. Ser. B Stat. Med.* **39**, 1–38 (1971).
41. Lewontin, R. The interaction of selection and linkage I. General considerations: Heterotic models. *Genetics* **49**, 49–67 (1964).
42. Hill, W.G. & Robertson, A. Linkage disequilibrium in finite populations. *Theor. Appl. Genet.* **22**, 226–231 (1968).

Am. J. Hum. Genet. 71:877–892, 2002

Neuregulin 1 and Susceptibility to Schizophrenia

Hreinn Stefansson,[1] Engilbert Sigurdsson,[2] Valgerdur Steinthorsdottir,[1] Soley Bjornsdottir,[1] Thordur Sigmundsson,[2] Shyamali Ghosh,[1] Jon Brynjolfsson,[2] Steinunn Gunnarsdottir,[1] Omar Ivarsson,[2] Thomas T. Chou,[1] Omar Hjaltason,[2] Birgitta Birgisdottir,[1] Helgi Jonsson,[2] Vala G. Gudnadottir,[1] Elsa Gudmundsdottir,[3] Asgeir Bjornsson,[1] Brynjolfur Ingvarsson,[3] Andres Ingason,[1] Sigmundur Sigfusson,[3] Hronn Hardardottir,[2] Richard P. Harvey,[4,5] Donna Lai,[4] Mingdong Zhou,[6] Daniela Brunner,[7] Vincent Mutel,[8] Acuna Gonzalo,[8] Greg Lemke,[9] Jesus Sainz,[1] Gardar Johannesson,[1] Thorkell Andresson,[1] Daniel Gudbjartsson,[1] Andrei Manolescu,[1] Michael L. Frigge,[1] Mark E. Gurney,[1] Augustine Kong,[1] Jeffrey R. Gulcher,[1*] Hannes Petursson,[2] and Kari Stefansson[1,*]

[1]deCODE Genetics and [2]Department of Psychiatry, National University Hospital, Reykjavík; [3]Department of Psychiatry, Akureyri Hospital, Akureyri, Iceland; [4]Victor Chang Cardiac Research Institute and [5]Faculties of Medicine and Life Sciences, University of New South Wales, Sydney; [6]Zensun Sci & Tech, Shanghai; [7]PsychoGenics, New York; [8]F. Hoffmann–La Roche, Basel, Switzerland; and [9]Molecular Neurobiology Laboratory, Salk Institute for Biological Studies, La Jolla, CA

The cause of schizophrenia is unknown, but it has a significant genetic component. Pharmacologic studies, studies of gene expression in man, and studies of mouse mutants suggest involvement of glutamate and dopamine neurotransmitter systems. However, so far, strong association has not been found between schizophrenia and variants of the genes encoding components of these systems. Here, we report the results of a genomewide scan of schizophrenia families in Iceland; these results support previous work, done in five populations, showing that schizophrenia maps to chromosome 8p. Extensive fine-mapping of the 8p locus and haplotype-association analysis, supplemented by a transmission/disequilibrium test, identifies *neuregulin 1* (*NRG1*) as a candidate gene for schizophrenia. *NRG1* is expressed at central nervous system synapses and has a clear role in the expression and activation of neurotransmitter receptors, including glutamate receptors. Mutant mice heterozygous for either *NRG1* or its receptor, *ErbB4*, show a behavioral phenotype that overlaps with mouse models for schizophrenia. Furthermore, *NRG1* hypomorphs have fewer functional NMDA receptors than wild-type mice. We also demonstrate that the behavioral phenotypes of the *NRG1* hypomorphs are partially reversible with clozapine, an atypical antipsychotic drug used to treat schizophrenia.

Introduction

Schizophrenia (MIM 181500) is a disabling brain disease affecting 0.5%–1% of the general population. It has a myriad of manifestations. These classically include one or more of the following: delusions, disordered thought, hallucinations, blunted emotions, paranoid ideation, and motor abnormalities such as stereotypic behaviors and catatonia (Liddle et al. 1994). More recently, other cognitive abnormalities—such as impaired memory, attention, and executive function—have been documented (Bilder 1996). Although there are medications that can alleviate some of these symptoms in patients, there is no cure available for schizophrenia, and most patients who respond to current treatments fail to cope fully in society.

Although conventional antipsychotics act by blocking dopamine receptors, there is considerable recent evidence linking defects in glutamatergic neurotransmission to the psychiatric manifestations of schizophrenia. Antagonists of glutamatergic signaling through the N-methyl-D-aspartate (NMDA) receptor (such as PCP, MK-801, and ketamine) induce psychosis in normal individuals and exacerbate manifestations of schizophrenia in patients. Recent studies have shown decreased binding to subunits of the glutamate receptor and decreased expression of subunits of the glutamate receptor in thalamic nuclei, hippocampus, and dorsal lateral prefrontal cortex of schizophrenic patients (Ibrahim et al. 2000; Gao et al. 2000). It is of interest that some of the atypical antipsychotics (such as clozapine) increase NMDA-receptor expression and directly facilitate glu-

Received June 20, 2002; accepted for publication July 9, 2002; electronically published July 23, 2002.

Addresses for correspondence and reprints: Dr. Hreinn Stefansson, deCODE Genetics, Sturlugata 8, IS 101-Reykjavik, Iceland; e-mail: hreinn@decode.is. Dr. Kari Stefansson, deCODE Genetics, Sturlugata 8, IS 101-Reykjavik, Iceland; e-mail: kstefans@decode.is. Prof. Hannes Petursson, Department of Psychiatry, National University Hospital, 101-Reykjavík, Iceland; e-mail: hannesp@landspitali.is.

* These authors contributed equally to this work.

0002-9297/2002/7104-0016$15.00

tamatergic transmission (Goff and Coyle 2001). Finally, mice with a reduced number of NMDA receptors exhibit behavior that overlaps that induced by PCP—hyperactivity, deficits in social interaction, and decreased prepulse inhibition (PPI); these are reversible with clozapine (Mohn et al. 1999). It is important to point out, however, that the glutamate dysfunction hypothesis is not incompatible with the dopamine hypothesis, because many reciprocal synaptic relationships exist between the two systems (Carlsson and Carlsson 1990).

Although the cause of schizophrenia is unknown, family and adoption studies suggest that schizophrenia has a significant genetic component (Cardno et al. 1999; Tsuang et al. 2001). As in most common diseases, the inheritance pattern is complex, and the penetrance is low. Unfortunately, there is no reliable biological marker for the disease. The many ways that schizophrenia manifests itself could be explained by locus heterogeneity, which also may have hampered progress in the search for schizophrenia genes. Given that neurotransmitter pathways are probably abnormal in schizophrenia, variants of genes encoding receptor subunits and transporters have been extensively tested for association to schizophrenia in many populations (O'Donovan and Owen 1999). Although there have been reports of weak association with variations of certain genes, no significant findings have been reproduced in independent cohorts. The associations reported so far, if real, represent only minor genetic contributions.

Numerous genomewide linkage scans have been reported for schizophrenia. There is modest evidence for linkage with several loci, including chromosome 1q, 2, 6, 8p, 13q, and 22q. The chromosome 8p locus (SCZD6 [MIM 603013]) shows suggestive linkage to schizophrenia in several different populations (Pulver et al. 1995; Kendler et al. 1996; Levinson et al. 1996; Blouin et al. 1998; Kaufmann et al. 1998; Shaw et al. 1998; Brzustowicz et al. 1999; Gurling et al. 2001). Information on the LOD scores and the *P* values in these studies is summarized by Brzustowicz et al. (1999).

Here, we present results of a genomewide scan for linkage to schizophrenia and a follow-up fine mapping at a locus on chromosome 8p. Haplotype analysis identifies *neuregulin 1* (*NRG1* [MIM 142445]) as a candidate gene for schizophrenia. Furthermore, we report functional studies supporting the notion that *NRG1* plays a role in the pathogenesis of schizophrenia. First, we confirm previous work (Gerlai et al. 2000) showing that mice hypomorphic for *NRG1* (with a different *NRG1* mutation than previously phenotyped) exhibit behavioral abnormalities. Second, we report that mice hypomorphic for the *NRG1* receptor, *ErbB4*, exhibit similar behavioral abnormalities. Third, we show that behavioral abnormalities of the *NRG1* hypomorphs can be partially reversed with clozapine. Fourth, our binding studies show that mice hypomorphic for *NRG1* have fewer functional NMDA receptors than do control mice, which is in keeping with observations made on brains from patients with schizophrenia (Ibrahim et al. 2000).

Subjects and Methods

Patients

This study was approved by appropriate ethics committees and the Data Protection Commission of Iceland (DPC). Informed consent was obtained from all patients and from their relatives whose blood and DNA samples were used in the linkage and association analysis. All personal identifiers associated with medical information and blood samples were encrypted by the DPC with a third-party encryption system, as described elsewhere (Gulcher et al. 2000). The genealogy database was encrypted by the DPC in the same manner. Taking part in the study were 476 patients—including 440 diagnosed with schizophrenia, 32 with schizoaffective disorder, and 4 with unspecified functional psychosis—as well as unaffected family members. Most probands were identified through referrals to the in- and outpatient services of all three psychiatric departments in Iceland (total population 285,000). Diagnoses were assigned according to Research Diagnostic Criteria (RDC) (Spitzer et al. 1978) through the use of the lifetime version of the Schizophrenia and Affective Disorders Schedule (SADS-L) (Spitzer and Endicott 1977). Psychiatrists who were blind to the genotyping data made consensus diagnoses.

Linkage Analysis

Large multiplex families were collected for the linkage scan. Pedigrees allowing for up to seven meiotic events between affected individuals were constructed, using a clustering algorithm, from an encrypted genealogy database that covers the entire Icelandic nation (Gulcher et al. 2000). A genomewide scan was performed using a framework map of 950 microsatellite markers and using protocols described elsewhere (Gretarsdottir et al. 2002). The marker order and positions for the framework mapping set were obtained from our high-resolution genetic map (Kong et al. 2002). We analyzed the data and determined statistical significance by applying a model independent affecteds-only allele-sharing method, implemented in the Allegro program, that calculates LOD scores on the basis of multipoint calculations (Gudbjartsson et al. 2000). Our baseline linkage analysis uses the S_{pairs} scoring function (Kruglyak et al. 1996), the exponential allele-sharing model (Kong and Cox 1997), and a family-weighting scheme that is halfway, on the log scale, between weighting each affected pair equally and weighting each family equally. In the analysis, we treat all genotyped individuals who are not affected as "un-

known." Affecteds are those who are diagnosed, using the RDC criteria, with schizophrenia, schizoaffective disorder, or unspecified functional psychosis.

Physical Mapping

The BAC contig of the region of interest, 8p11-p21, was generated using the RCPI-11 Human BAC library. BAC identification and contig orders were determined by hybridization using available STS markers and microsatellite markers in the region, followed by successive rounds of hybridization using markers designed from BAC end sequences. BAC fingerprint data complemented these data. Fingerprints of positive clones (FPCs) were analyzed using the FPC database developed at the Wellcome Trust Sanger Institute. New microsatellite markers were discovered from cloning and by screening fragments from nebulized BACs.

Identification of At-Risk Haplotypes

To handle missing genotypes and uncertainty with phase, our own implementation of a likelihood approach, using the expectation-maximization (EM) algorithm (Dempster et al. 1977) as a computational tool, was applied to estimate the haplotype frequencies. Under the null hypothesis, the affected individuals and controls are assumed to have identical frequencies of all haplotypes. Under the alternative hypothesis, the candidate at-risk haplotype is allowed to have a higher frequency in affected individuals than controls, while the ratios of the frequencies of all other haplotypes are assumed to be the same in both groups. Likelihoods are maximized separately under both hypotheses and a corresponding 1-df likelihood ratio statistic is used to evaluate statistical significance. While our own computer program was developed to fit our chosen models, and to handle missing genotypes and haplotypes with many markers efficiently, our use of the EM-algorithm is very similar to methods used by others (Excoffier and Slatkin 1995; Hawley and Kidd 1995; Long et al. 1995). Although applied in a slightly different setting, the 1-df model we use is essentially that used by Clayton and Jones (1999).

Transmission/Disequilibrium Test

The transmission/disequilibrium test (TDT) was performed on probands for whom both parents are genotyped, and one or both parents are heterozygous for the at-risk haplotype (Spielman et al. 1993).

Sequencing of the NRG1 *Locus and Identification of Exons and Transcripts*

BACs covering the minimum tiling path of the region of interest were analyzed by shotgun cloning and sequencing (GenBank accession numbers AF491780 and TPA BK000383). Dye terminator (ABI PRISM BigDye) chemistry was used for fluorescent automated DNA sequencing. ABI Prism 377 sequencers were used to collect data, and the Phred/Phrap/Consed and Polyphred software packages were used to assemble sequences. We identified syntenic mouse BACs (library RPCI-23), and, by BAC walking, a contig across the *NRG1* locus was made. The methods described above were used to subclone and sequence eight syntenic BAC clones from the mouse. The mouse sequence was used to identify more exons and potential regulatory elements. Both 3′ and 5′ RACE (rapid amplification of cDNA ends) were performed using the Marathon-Ready cDNA from Clontech Laboratories and cDNA libraries made at deCODE genetics. cDNA libraries from whole brain, fetal brain, and testis were screened.

Exon trapping was performed using Exon trapping system (Live Technologies). Primers were designed for amplification of candidate exons from cDNA libraries, touchdown PCRs were performed, and products were verified by sequencing.

Search for SNPs

Exons were screened by direct sequencing from a PCR template. Exon sequences and sequences 2 kb upstream of each transcription start site from 184 patients were analyzed for SNP detection. Conserved regions within the 1.5-Mb *NRG1* locus sequence (potential regulatory elements) showing ≥80% mouse:human identity over ≥100 bp were screened in 94 patients. SNPs were scored using a fluorescent-based method (Chen et al. 1999).

Mouse Phenotyping

NRG1 transmembrane-domain–knockout mice were generated using a targeting vector in which most of exon 11, which encodes the transmembrane domain, and some of the immediate downstream intron were replaced with a neomycin resistance gene cassette, preceded by an oligonucleotide carrying stop codons in each reading frame and a polyadenylation sequence. The targeting vector was electroporated into J1 embryonic stem (ES) cells (129/terSv), and founding chimeras were outcrossed to C57Bl/6 mice to establish the line. Heterozygous mice were healthy and fertile, although homozygous embryos died of cardiac defects around E10.5–E11.5. These mice will be described more fully elsewhere (R. P. Harvey, D. Lai, and M. Zhou, unpublished data). *ErbB4* hypomorphic mice heterozygous for a null allele of the gene were generated by replacement of the coding region of exon 2 with a reporter gene (Gassmann et al. 1995). Heterozygous null *NRG1* and *ErbB4* mice were bred at Charles River Laboratories by crossing to a C57Bl/6 background. Six weeks prior to behavioral testing, male mice and litter-mate control mice for each line were

shipped to the testing laboratory at PsychoGenics, where they were housed in groups of three to five related mice per cage.

The open-field study was conducted when the male mice were 5–6 mo of age. Group-housed mice were brought into the experimental room and were allowed to acclimate for 1 h prior to testing. Each mouse was placed for 30 min in a square open-field box (17 × 17 × 12 inches). Up to eight animals were tested at one time, with one animal in each of eight arenas, under low lighting conditions (provided by a 15-W red lamp). The automated infrared beam array system measured locomotion in the center and periphery of the test arena. Activity data were collected in 5-min intervals over the 30-min open-field session and were analyzed with a series of repeated-measures analysis of variance (ANOVA), with session interval as a within-subject factor and genotype as a between-subject factor. Clozapine (1 mg/kg in 1% Tween 20, pH 6.0) was injected intraperitoneally (i.p.) 25 min before behavioral testing. Total activity data from the study with clozapine were analyzed with a two-tailed Student's *t* test. Experimentally naive mice were used for these experiments. It seemed that handling the mice or habituation to the testing conditions changed the level of hyperactivity or the sensitivity to clozapine on repeated testing.

The cross maze consisted of an eight-arm radial arm maze with four of the arms blocked. The maze was placed on the floor of a dimly lit room (one 25-W lamp) that had contrasting cues on the wall and on the outside of the blocked arms of the maze. Each arm measured 14 inches long × 3 inches wide, and the center hub measured ~8.5 inches in diameter. Wild-type and heterozygous mice were individually placed and tested in the cross maze for 8 min. Global activity was reflected in the total number of visits to the different arms. A visit to an arm was recorded when the body of the mouse crossed the dividing line between the hub and the arm. The number of visits to each arm and the order of arm visits were recorded. Percentages of triple and quadruple alternations were calculated, where a triple alternation was the visit of three different arms without entry into any arm already visited, and quadruple alternation was the visit to four arms without re-entry (e.g., A-B-C-D, A-D-C-B, etc., where the letters refer to the arms of the maze). The percentage was obtained by comparison of the number of triple or quadruple alternations against the number of possible triple or quadruple visits.

For assessment of PPI, group-housed mice were brought into the experimental room and were allowed to acclimate for a minimum of 1 h prior to testing. Mice were individually placed in a startle enclosure in the startle chamber with a background white noise of 70 dB and were left undisturbed for 10 min. Then a 16-min session was started that consisted of 56 trials. Each trial started with a 50-ms null period, followed by a 20-ms prepulse white noise of 72, 74, or 78 dB. After a 100-ms delay, the startle stimulus was presented (a 40-ms 120 dB white noise), followed by a 290-ms recording time. The total duration of the trial was 500 ms. Eight types of trials were given: prepulse (72, 74, or 78 dB) plus startle (10 trials per prepulse intensity), prepulse (72, 74, or 78 dB) alone (4 trials per prepulse intensity), startle alone (10 trials), and no stimulation (4 trials). The variable intertrial interval averaged 15 s (range 10–20 s). In the no-stimulation trials, baseline measurements were taken. In the startle-alone trials, the basic auditory startle was measured, and, in the prepulse-plus-startle trials, the amount of inhibition of normal startle was measured and was expressed as a percentage of the basic startle. In the prepulse-alone trials, the normal response to a weak noise was measured as a control. Data from trials in which the latency to the peak amplitude of the startle was >80 ms were excluded from the analysis. Animals with a mean startle <100 units were also excluded from the analysis.

[^3H] *MK-801 Binding Sites*

[^{3}H]-dizocilpine (MK-801) binding in *NRG1* hypomorphic mice (Gerlai et al. 2000) and control mice was studied as follows: Wild-type (n = 18), and *NRG1* mutant mice (n = 16) forebrains were homogenized individually at 4°C in 25 volumes of Tris-HCl 50 mM, EDTA 10 mM, pH 7.1 buffer with a polytron (10,000 rpm, 30 s). The homogenate was centrifuged at 48,000 *g* for 10 min, and the pellet was rehomogenized as above and was incubated for 10 min at 37°C. After centrifugation, the pellet was homogenized as above, and the homogenate was frozen at −80°C. [^{3}H]-dizocilpine saturation isotherms were obtained by incubation of various amounts of the radioligand (0.1–100 nM, final concentration) in the presence of 10 mg brain membranes for 2 h at room temperature in a Tris-HCl 5 mM, glycine 100 μM, glutamate 100 μM, pH 7.4 binding buffer. The nonspecific binding was measured in the presence of 100 μM 1-[1-(2-thienyl)cyclohexyl]piperidine (TCP). After incubation, the membranes were filtered on GF/B glass-fiber filters preincubated for 1 h in a polyethylenimine 0.1% solution. The filters were washed three times with 3 ml of cold binding buffer, and the radioactivity bound to the membranes was measured by liquid scintillation counting. The binding parameters K_D and B_{max} were obtained from the fit to the data of the equation of a rectangular hyperbola (one-site model) by nonlinear regression and were analyzed by ANOVA.

Results

Schizophrenia Mapped to Chromosome 8p12-p21

The 33 families used for linkage consist of 110 patients, 105 of whom were available for genotyping. The

highest initial multipoint LOD score was 3.06, on chromosome 8p at marker D8S532 (fig. 1). Linkage to 8p has been reported by a number of groups, working with different populations (Pulver et al. 1995; Kendler et al. 1996; Levinson et al. 1996; Blouin et al. 1998; Shaw et al. 1998; Kaufmann et al. 1998; Brzustowicz et al. 1999; Gurling et al. 2001). The region we find to have the highest LOD score on 8p is 10–15 cM centromeric to most previously reported linkage to 8p. Low marker density, low resolution of linkage studies, and uncertainty with maps in many of the older studies may account for this difference. The work reported here was done utilizing a high-resolution genetic map that was not available to the other studies (Kong et al. 2002). It is, however, possible that this is a distinct locus.

The 8p12-p21 locus was physically mapped using BACs. The primary goal with the BAC map was to achieve a high-resolution ordering (100–150 kb) of all polymorphic markers in a 30-cM region and to facilitate the search for new polymorphic markers. After adding extra markers within the linkage peak, thus increasing the information content, the peak allele-sharing LOD score for the 33 families declined from 3.06 to 2.53 at D8S278 (fig. 2). The corresponding multipoint para-

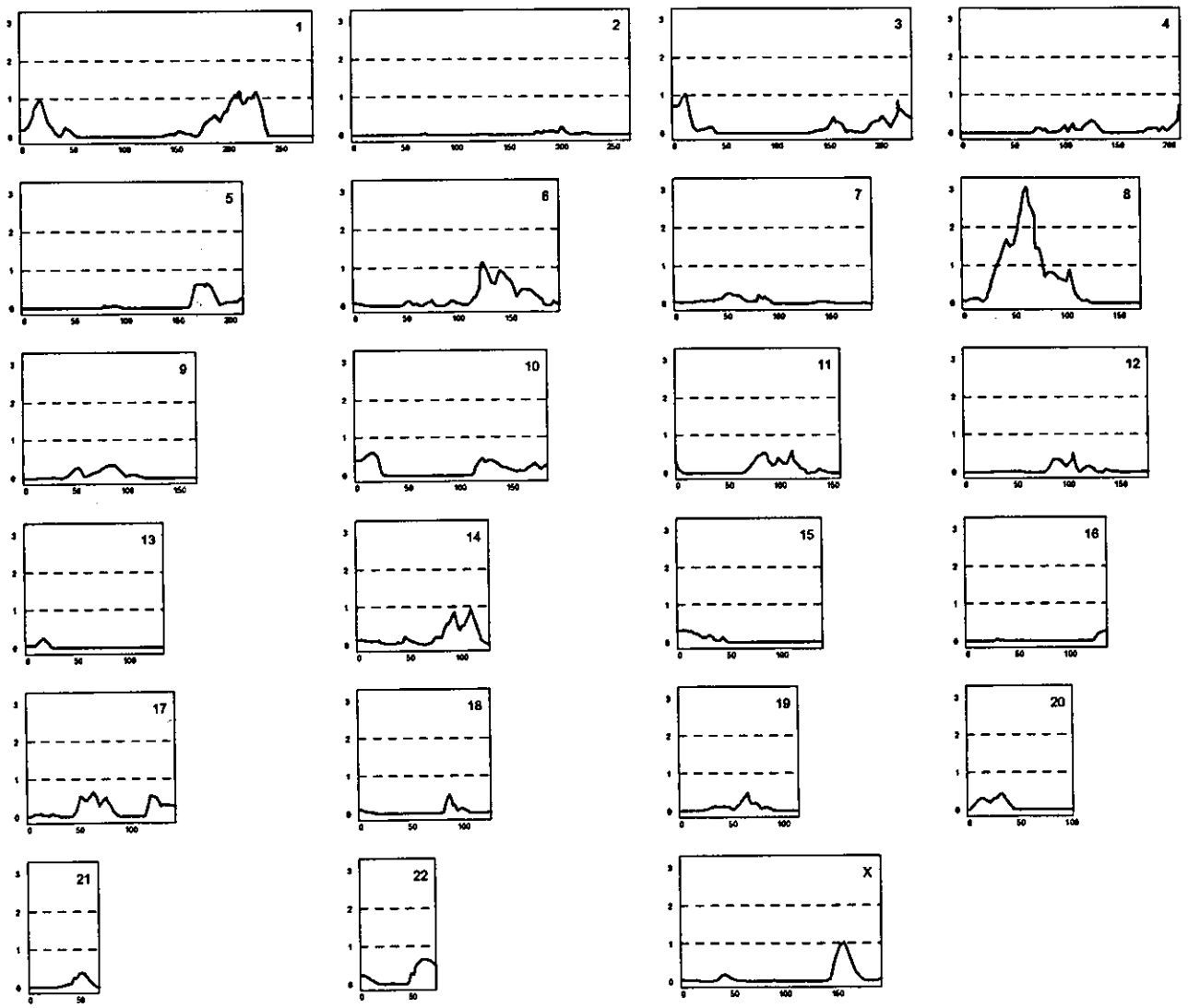

Figure 1 Genomewide scan of 110 patients with schizophrenia from 33 families. The 110 patients included 106 who fulfilled the Research Diagnostic Criteria (RDC) schizophrenia diagnosis, three patients diagnosed with unspecified functional psychosis, and one diagnosed with schizoaffective disorder. With the assistance of our genealogical database, the patients were clustered into 33 families, and relations between patients are as distant as second cousins. The patients and their relatives were genotyped using a framework set of 950 microsatellite markers. The *X*-axis gives the genetic distance (in cM) along the chromosome, and the *Y*-axis gives the LOD score. The data were analyzed using multipoint allele-sharing, without specification of an inheritance model, using Allegro (Gudbjartsson et al. 2000).

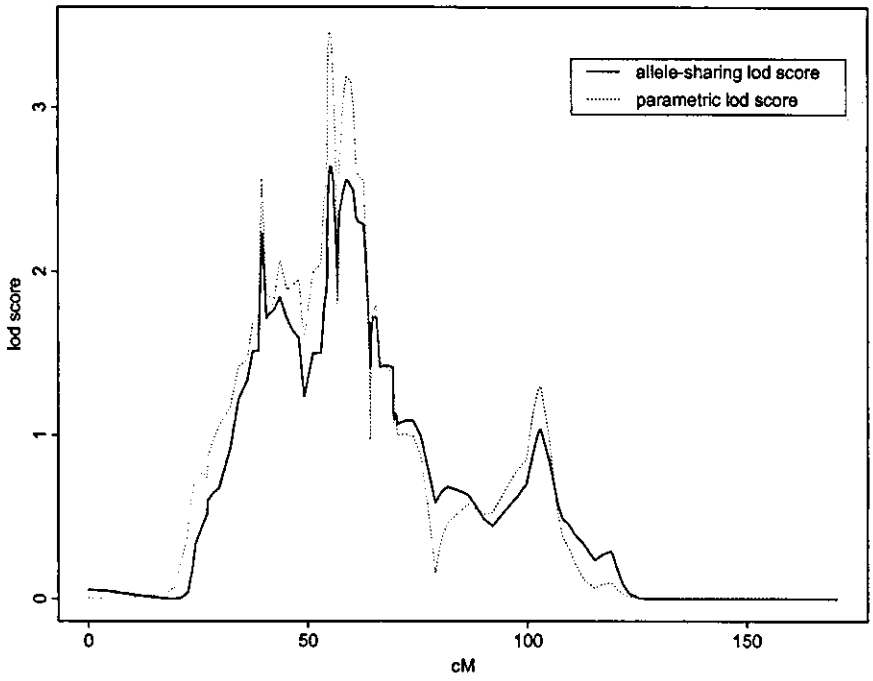

Figure 2 Fine mapping of the schizophrenia locus on chromosome 8p, with 50 additional markers mapped to the 30-cM locus. Since correct marker order and genetic distance is essential for multipoint genetic analysis, we determined the order of markers by generating a physical map of 30 cM in 8p12-p21, using BAC clones, and we determined the genetic distances on our high-resolution genetic map, on the basis of 1,200 meiotic events (Kong et al. 2002). The solid line represents the allele-sharing LOD score, and the dashed line represents the parametric LOD score. The additional markers increased the information content from 0.7 to >0.9. The *X*-axis gives the genetic distance (in cM) along the chromosome, and the *Y*-axis gives the LOD score.

metric LOD score was 3.48 when an affecteds-only multiplicative model was used (i.e., an allele frequency of 0.03 and a six-fold risk, relative to the wild-type, for every at-risk allele carried). These results constitute only suggestive linkage to chromosome 8p, but, along with results of previous studies, they convinced us to search for haplotypes in this region to assess for association with schizophrenia.

Haplotype Analysis Identifies NRG1 *as a Candidate Gene for Schizophrenia*

We increased the density of microsatellite markers further at the 8p locus, to achieve an average density of 1 marker every 75 kb within a 5 cM region centered on D8S278. For the linkage families, we examined all patient haplotypes shared identical by descent by multiple patients within a family, and then we compared these haplotypes across families. Two such haplotypes, each appearing in multiple families, are shown in figure 3: microsatellite haplotypes I and II. Shared haplotypes between families carrying microsatellite haplotype I pointed us to an ~600-kb region (fig. 3). To validate the relevance of the two haplotypes identified and to further narrow down the region, 373 additional patients were collected and genotyped, in addition to the patients used in the linkage analysis. Many of these additional patients had sporadic disease, or their affected relatives were not alive, but a fraction of the patients were related. In parallel, we identified, from our physical map, BACs covering the at-risk haplotypes (fig. 3) and sequenced them by a shotgun approach, covering a total of 1.2 Mb, to search for genes within the region (GenBank AF491780). Within the boundaries of the at-risk microsatellite haplotypes, we found a *5′* exon from the *NRG1* gene and an EST cluster with unknown function, *Hs.97362* (fig. 3). We have submitted the complete sequence of the large *NRG1* gene to GenBank (accession number TPA BK000383).

Furthermore, we sequenced the syntenic mouse locus, 1.2 Mb in size, to help identify exons and regulatory elements. In figure 3, the exon-intron structure of the two genes is shown schematically, together with the overlapping at-risk microsatellite haplotype I. In the search for novel exons and genes, we used RT-PCR, 3′ and 5′ RACE, and exon trapping from BACs covering the *NRG1* gene and 200 kb of the upstream sequence. Novel exons and splice variants were identified for both genes (H. Ste-

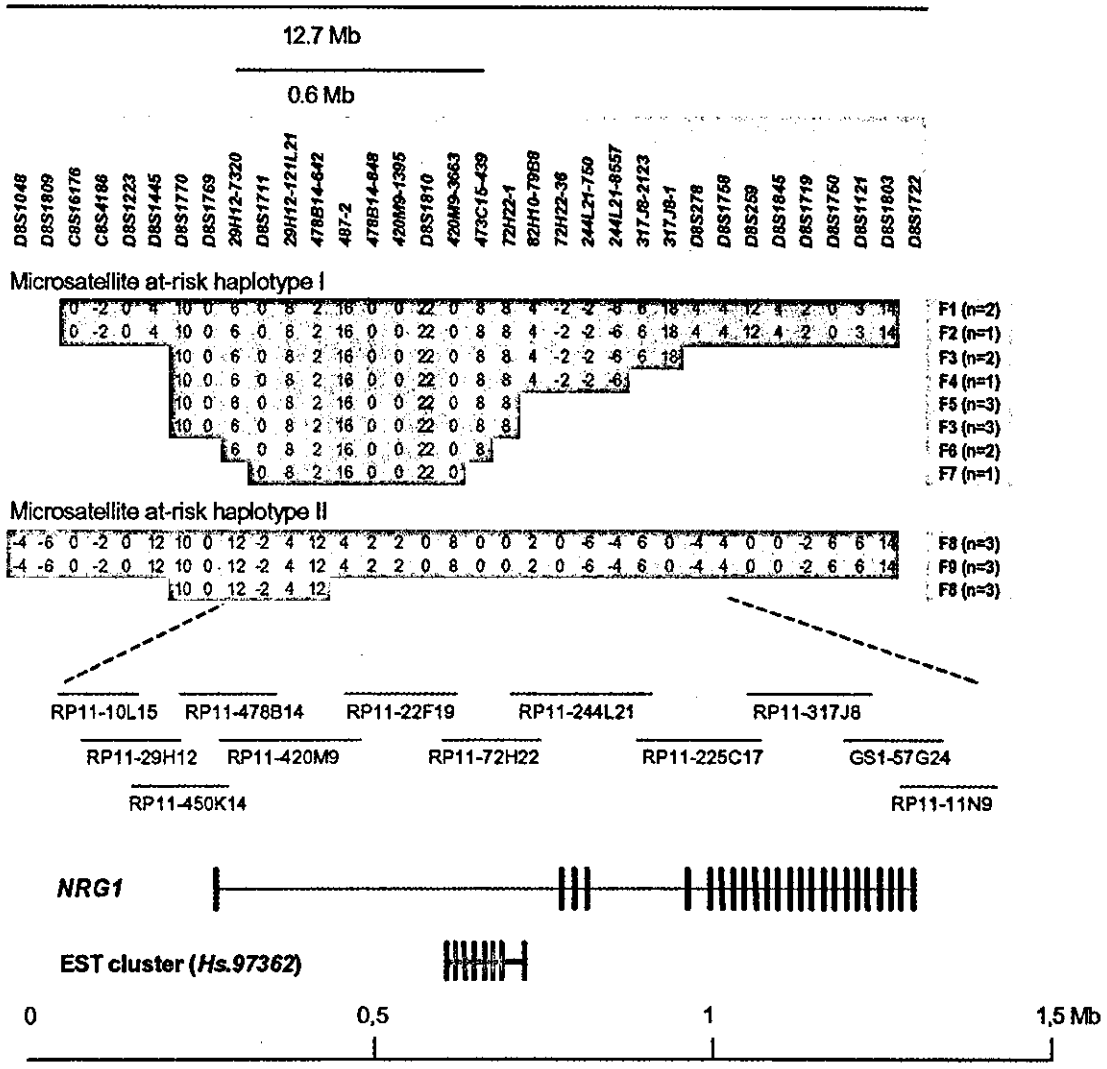

Figure 3 Microsatellite at-risk haplotypes on chromosome 8p and known genes within a region showing haplotype sharing between 9 of the 33 linkage families. Extensive sharing of two microsatellite haplotypes between patients from the linkage families is shown at the top. Haplotypes were reconstructed by application of the Allegro program (Gudbjartsson et al. 2000), using available family members to derive the phase. Key markers in the haplotypes are shown, and the size of the region is indicated. Families carrying the haplotypes are labeled F1–F9, and the number of affected individuals in each family carrying that haplotype is given in parentheses. Maximum haplotype sharing between families is 9.5 Mb for haplotype I and 11.4 Mb for haplotype II. Shared haplotypes between families narrow the region of interest to 600 kb between markers *29H12-7320* and *473C15-439*, indicated by a bar (microsatellite haplotype I). The location of a BAC contig covering 1.5 Mb of the locus region is indicated. The sequence of GS1-57G24 was obtained from the public domain (GenBank accession number AF128834), but we sequenced the other BACs shown. The positions of *NRG1* and an EST cluster of unknown function (*Hs.97362*) are schematically shown in relation to the BACs. Exons are indicated by vertical bars.

fansson, V. Steinthorsdottir, J. R. Gulcher, and K. Stefansson, unpublished data).

In an attempt to identify causal alleles, we have screened all known and novel exons of *NRG1* ($n = 25$) and EST cluster *Hs.97362* ($n = 8$) and have identified 15 nonsynonymous SNPs for *NRG1* and 3 in the EST cluster *Hs.97362*. We have identified two synonymous SNPs and seven SNPs in the untranslated part of *NRG1* and one synonymous SNP and four SNPs in untranslated regions of EST cluster *Hs.97362*. A total of >1,200 SNPs have been identified in the entire *NRG1* sequence (see deCODE Genetics Web site). All coding SNPs and a number of SNPs in promoter regions were genotyped for 394 unrelated control individuals and 478 patients. Furthermore, a number of SNPs identified in conserved regions were also scored. A total of 58 SNPs were genotyped for all

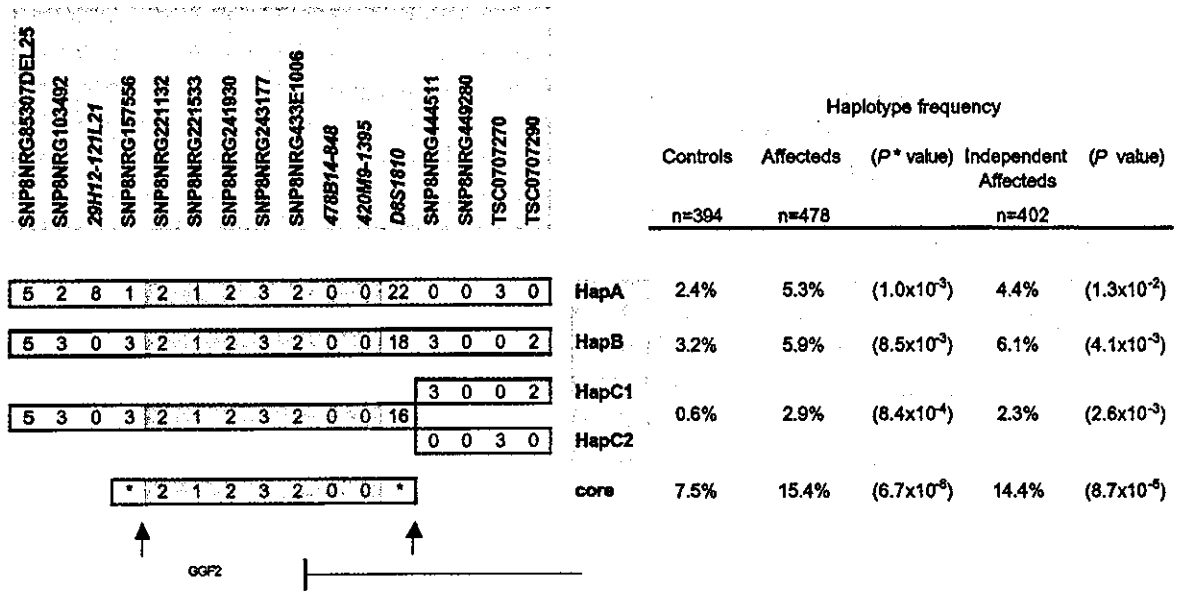

Figure 4 Microsatellite and SNP at-rick haplotypes at the 5′ end of the *NRG1* gene. Four haplotypes, defined by 12 SNPs and four microsatellite markers, were individually found in excess in the schizophrenia patients with similar relative risk. The common core for these haplotypes, defined by five SNPs and two microsatellite markers, is shown at the bottom. The frequencies for each haplotype in all affected individuals, independent affected individuals, and control individuals are indicated in the panel on the right. The only known exon within the boundaries of the core at-risk haplotype is the 5′ exon of GGF2, as indicated in the figure. The distance between the markers flanking possible recombination breakpoints (*arrows*) is 290 kb, corresponding to 0.16–0.45 Mb on the scale at the bottom of figure 3.

patients, and, in a subset of patients (n = 94) and control individuals (n = 124), an additional 123 SNPs were scored for association. A few SNP alleles showed mild but significant single-marker associations, but they do not change amino acids or splice sites.

Haplotype analysis was performed as described in the "Subjects and Methods" section. Unless otherwise stated, P values reported for association tests are one-sided, without adjustment for multiple comparisons, and are based on the EM algorithm. Also, the likelihoods are computed treating all affected individuals as independent. If the affected list includes related individuals, the estimates of haplotype frequencies are still valid, whereas the P values calculated would be slightly anticonservative. We indicate all such P values with an asterisk (*). From the list of all affected individuals, a smaller list of independent affected individuals is created, blind to the genotypes, by eliminating first- and second-degree relatives. Although the P values computed from such a reduced list is valid, the frequency of a haplotype that is shared by many affected relatives tends to be underestimated. We have also used other methods, including the Allegro program (Gudbjartsson et al. 2000), to construct the most likely haplotypes on the basis of patients and relatives, with comparable results.

No single SNP marker or microsatellite marker was very statistically significant or had very high estimated relative risk. The SNP giving the best uncorrected single-marker association was SNP8NRG221533 (P = .003). However, a core haplotype consisting of five SNPs (including SNP8NRG221533) and two microsatellite markers was identified (P value between 6.7×10^{-6}* and 8.7×10^{-5}) (fig. 4). Four of the SNP markers are upstream of the *NRG1* gene, but the fifth one (SNP8NRG433E1006) is coding, changing an arginine to a glycine in the 5′ exon of glial growth factor 2 (GGF2), which is one of many splice forms of *NRG1*. However, the common variant, which is glycine (found in 88% allelic frequency in case individuals and 85% in control individuals), is associating with the core at-risk haplotype and therefore not likely by itself to be the causative allele. Information on sequence of SNPs and microsatellites within the *NRG1* sequence can be found at the deCODE Genetics Web site. The core haplotype covers 290 kb and represents a block of linkage disequilibrium containing the first 5′ exon of *NRG1*, encoding for the amino terminus of GGF2, and upstream sequences. Close to 90% of this core haplotype can be accounted for by four extended haplotypes involving 16 markers (fig. 4). Interestingly, whereas HapA in figure 4 corresponds to the extended microsatellite haplotype I in figure 3 identified in the linkage families, HapB and HapC (1 and 2), apart from having common alleles for microsatellite markers *478B14-848* and *420M9-1395*,

tend to have different alleles for many of the microsatellite markers (not all shown in fig. 4). Indeed, at various intermediate stages before we realized that they share a core, HapA, HapB, and HapC (1 and 2) were each considered as independent at-risk haplotypes showing significant excess in the patients relative to the control individuals (fig. 4). The estimates of their risks, relative to the wild type, are also comparable for HapA and HapB (relative risk ~2) and are higher for HapC, but the estimate for HapC is based on small numbers (fig. 4). Hence, we believe that this core haplotype is capturing an ancestral at-risk haplotype that is represented by a number of extended microsatellite/SNP haplotypes in the current population. For the seven markers, that define the core at-risk haplotype in figure 4, there are only 15 distinct haplotypes with frequencies > 1% (frequencies estimated under the null hypothesis with the data from the patients and controls combined), together accounting for 56% of the haplotypes in the population. There are 65 distinct haplotypes with estimated frequencies >0.1%, together accounting for 94% of haplotypes.

Figure 4 shows the likely locations of historic recombination breakpoints and also reveals that the microsatellite marker *D8S1810* has probably mutated since the at-risk SNP haplotype was formed. Haplotypes derived using information from relatives of patients and controls agreed with these haplotypes derived using the likelihood approach.

The core at-risk haplotype has an estimated frequency of 7.5% in the general population and of 15.4% among all patients with schizophrenia. When a multiplicative model is assumed, affected individuals are estimated to have 2.2 times the risk of the wild type for each at-risk haplotype evaluated. To supplement the results from the case-control study, we performed the transmission/disequilibrium test (Spielman et al. 1993) and found that, for parents who were heterozygous with respect to the core haplotype, there were 33 transmissions to the affected offspring and 17 nontransmissions ($P = .016$). Although these results are only marginally significant, because of the small sample size (parents were not available for genotyping in many cases), it is heartening that the ratio of transmissions to nontransmissions is close to 2:1, which is consistent with the relative risk of 2.2 estimated on the basis of the case-control data.

It is worth noting that the region of interest exhibits extensive linkage disequilibrium. The core haplotype of seven markers can be identified by only three markers, one SNP and two microsatellites. Specifically, if a haplotype includes alleles 1, 0, and 0 for SNP8NRG221533, *478B14-848*, and *420M9-1395*, respectively, then there is little uncertainty that it has the corresponding alleles for the other four markers. Moreover, HapA, HapB, and HapC in figure 4 each can be captured by only five markers, the three identifying the core plus microsatellite markers *29H12-121L21* and *D8S1810*. Also, HapA is a good surrogate for the extended microsatellite haplotype I in figure 3. The core at-risk haplotype does not overlap with EST cluster *Hs.97362*, suggesting that *NRG1* is the more likely candidate gene in this region. The EST cluster is 103 kb centromeric to marker TSC0707290 shown in figure 4. None of the five SNPs defining the core haplotype is likely to be the causative SNP, since they do not individually capture the same degree of association as the core haplotype, they are, therefore, more likely in linkage disequilibrium with a causative allele, within the boundaries of the core at-risk haplotype. Although we have screened 20 kb of the 290-kb core at-risk haplotype for SNPs, including the known exon and regulatory elements within the core, there may remain regulatory elements we have not identified, containing a functional variant that may affect transcription, RNA splicing, RNA stability, RNA transport, or translation. Alternatively, the functional variant may include more than one polymorphic site, and a haplotype may be necessary to account for the susceptibility, as has been suggested for other complex diseases (Drysdale et al. 2000; Horikawa et al. 2000). Finally, this may represent large or small inversions, deletions, or duplications that have not been uncovered by our mutational analysis so far.

Microsatellite haplotype II (fig. 3) was found in substantially higher frequency in patients from the linkage families than in control individuals (data not shown). The markers identifying this haplotype overlap with those of the core haplotype shown in figure 4, but the alleles are different. This haplotype is rare in control individuals and in the patients who were not used in the linkage analysis. Hence, we can currently neither confirm nor reject this haplotype as conferring increased risk.

On the basis of the estimated frequencies and relative risks reported above, the core haplotype has a population attributed risk of 16% when the multiplicative model is used. It accounts for a 9% increase in risk for siblings of an affected individual. Hence, its contribution to the familial risk of schizophrenia, which has been reported to have λ_s close to 8.6 (Risch 1990), is small and cannot fully explain the linkage results we and others obtain for this region. Although part of the reason could be that there are other schizophrenia susceptibility genes in the 8p region contributing to the LOD scores and results from linkage analyses have a tendency to overestimate the contribution of the gene (Goring et al. 2001), we believe there must be other at-risk alleles/haplotypes of *NRG1*, probably rarer but possibly with higher penetrance, yet to be found (e.g., microsatellite haplotype II). Hence, the overall contribution of *NRG1* to schizophrenia may be substantially higher than the estimate reported here.

NRG1 *and* ErbB4 *Mutant Mice Display Behavioral Abnormalities*

Schizophrenia is one of the diseases affecting higher cortical functions for which it has been difficult to develop an animal model that comes close to the human disease. Indeed, many of the clinical manifestations of schizophrenia affect mental processes that draw a line of distinction between humans and other animals. Conventional antipsychotic drugs can be evaluated in rodents, using behavioral assays sensitive to dopaminergic tone (such as locomotion), yet these have no clear correspondence in the schizophrenic patient. The rank order of potency of such drugs shows a relatively good correlation between inhibition of dopamine-receptor binding and clinical benefit (Creese et al. 1976). In addition to altering dopaminergic function, the newer class of atypical antipsychotic drugs (e.g., clozapine) have potent effects on other neurotransmitter systems, including serotonin.

NRG1 and its receptors, *ErbB2, ErbB3,* and *ErbB4,* are essential genes for development (Gassmann et al. 1995). Homozygous null embryos die at 10.5–11 d of gestation or soon after birth. Heterozygous null mice, in contrast, are viable and live to adulthood (Gerlai et al. 2000). *NRG1* hypomorphic mice show hyperactivity in a number of tests, including the novel open field and alternating-Y maze, whereas *ErbB2* and *ErbB3* heterozygous null mice are behaviorally normal. The *NRG1* mutant mice used in these studies were generated by a disruption of the gene targeted so that the epidermal growth factor (EGF)–like domain is missing (Erickson et al. 1997). To replicate the abnormal behavioral results of the reported *NRG1* mutant mouse, we carried out behavioral studies on a second line of *NRG1* heterozygous mice (in which the targeted deletion was of exon 11, encoding the *NRG1* transmembrane domain [R. P. Harvey, D. Lai, and M. Zhou, unpublished data]). We also studied a line of *ErbB4* heterozygous null mice (Gassmann et al. 1995). Quantitation of *NRG1* and *ErbB4* mRNA in hippocampus, performed using RT-PCR, confirmed that 50% reduction of message from the targeted genes was achieved in both lines of mice.

The *NRG1* and *ErbB4* heterozygous null mice bred well, developed normally, and showed generally normal behavior. The lines were maintained by back crossing onto C57Bl/6 but were not congenic. When evaluated in the novel open-field test performed under dim red light, both types of mice were significantly more active than their wild-type litter-mate controls, with whom they had been housed since weaning (figs. *5a* and *5b*). Because mice are neophobic and find open spaces aversive, normal mice will prefer to stay close to the walls (thigmotaxis), and, indeed, there was no difference between *NRG1* or *ErbB4* hypomorphs and their normal litter-mate controls in measures of anxiety, such as time spent in the center of the test arena. Hyperactivity in the novel open-field test was more robust in the *NRG1* hypomorphs than in the *ErbB4* hypomorphs. Hyperactivity of the *NRG1* hypomorphs also was seen in a four-arm–cross maze test. This is an ethologically based test that assesses exploratory activity in a novel environment but does not involve reward delivery. The total number of entries into one of the four arms of the maze was increased (37 ± 1.7 vs. 30 ± 1.6, F-test; $P = .01$). The mice were otherwise behaviorally normal, with no difference between genotypes in patterns of quadruple or triple alternations or clockwise or counterclockwise patterns of entry. That the hyperactivity was more robust in the *NRG1* hypomorphs than in the *ErbB4* mutant mice may indicate that the ligand is limiting in the *NRG1/ErbB4* signaling pathway.

Hyperactivity is seen in a number of mutant mice, particularly those showing an increase in dopaminergic tone, such as the dopamine transporter (DAT) null mice (Glickstein and Schmauss 2001), the muscarinic acetylcholine–receptor M1 subtype null mice (Gerber et al. 2001), and N-methyl-D-aspartatereceptor subunit NR1 hypomorphic mice (NR1 mice) that express only 10% of the normal level of NR1 (Mohn et al. 1999). In both the DAT and NR1 mutants, the hyperactivity is reversible with antipsychotic drugs. Drugs such as clozapine are sedating at high doses, but, at doses of ≤ 1 mg/kg, they will reverse the hyperactivity in mutant or pharmacologic models of schizophrenia but will have no effect on spontaneous activity (O'Neill and Shaw 1999). To explore reversibility of the hyperactivity of the *NRG1* hypomorphs in the two behavioral assays, we tested the effect of clozapine at a dose of 1 mg/kg on the *NRG1* hypomorphs and their normal litter-mate controls. Clozapine at the dose chosen reversed the increased activity of the *NRG1* hypomorphic mice in the novel open-field test (*t*-test, $P < .02$) (see insert in fig. *5a*). Clozapine had no effect on the spontaneous activity of normal mice in the novel open field and thus was not sedating at that dose. In the cross maze test, clozapine at 1 mg/kg also reversed the hyperactivity of the *NRG1* hypomorphs. The total number of entries by the *NRG1* hypomorphs was reduced to baseline in the clozapine-treated animals (from 36.9 ± 4 in vehicle-treated animals to 27 ± 2 in clozapine-treated animals; $P = .03$), whereas clozapine had no significant effect on the spontaneous activity of normal litter-mate control mice in the cross-maze test.

PPI

Although locomotory assays in rodents may have validity as pharmacologic models for the evaluation of antipsychotic drugs affecting dopaminergic tone, their direct clinical correlate in the schizophrenic patient is

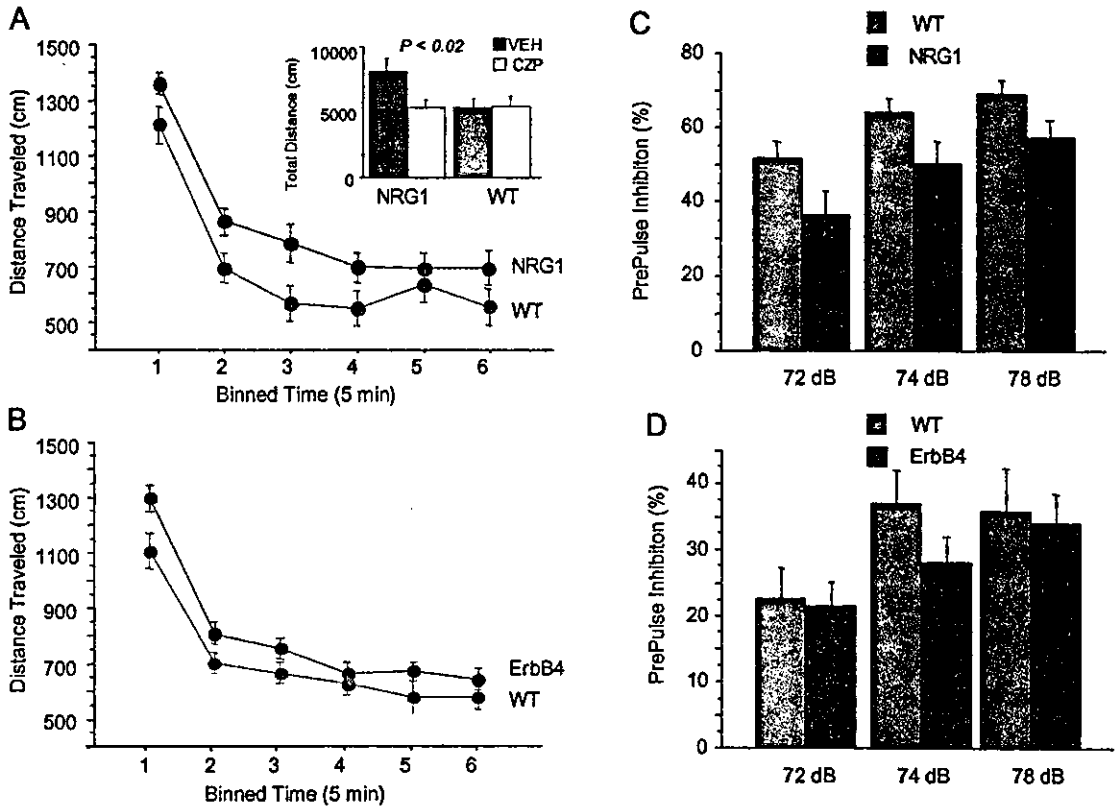

Figure 5 Locomotion and PPI in *NRG1* and *ErbB4* hypomorphic mice. *NRG1* and *ErbB4* hypomorphic mice were significantly more active, according to different measures that reflect locomotion and exploration. Here, we show distance traveled in a novel open-field test for the two lines of mice: *NRG1* hypomorphic mice (*A*) and *ErbB4* hypomorphic mice (*B*). Data have been binned into 5-min intervals over the 30-min observation period. Distance traveled was significantly increased in both *NRG1* and *ErbB4* male mice in comparison to litter-mate control mice (n = 21 *NRG1* mice and 22 litter-mate control mice, P = .04; n = 39 *ErbB4* mice and 22 litter-mate control mice, P = .03). Open-field activity was monitored as described. Error bars indicate the SEM. *A, insert,* hyperactivity of the *NRG1* mutant mice was reversed by clozapine. The *NRG1* mice and litter-mate control mice were injected i.p. with either clozapine (1 mg/kg) or vehicle, 25 min prior to testing (n = 10 *NRG1* mice and 10 control mice, P = .02). Open-field activity was monitored as described in the "Subjects and Methods" section. PPI was recorded for *NRG1* (*C*) and *ErbB4* (*D*) hypomorphic mice, using a conditioning, prepulse noise burst of 72, 74, or 78 dB. *NRG1* hypomorphic mice have impaired PPI in comparison to normal, litter-mate control mice (F-test, P = .03), whereas *ErbB4* mutant mice were not significantly impaired (F-test, P = .056).

unclear. On the other hand, a number of studies indicate that some schizophrenic patients have impaired PPI. This is a psychometric measure of sensory gating that can be evaluated in similar fashion in rodents and humans (Braff and Geyer 1990). We find that PPI is impaired in the *NRG1* hypomorphic mice and less so in the *ErbB4* mutant mice. The auditory/perceptual systems of *NRG1* and *ErbB4* hypomorphic mice are generally intact, since both show normal acoustic startle responses to a single noise burst of 120 dB. With respect to PPI, however, *NRG1* hypomorphic mice were impaired in comparison to normal litter-mate controls (F-test, P = .03) (fig. *5c*). However, the *ErbB4* hypomorphs did not show significant difference in PPI (F-test, P = .056) (fig. *5d*). The defect in PPI in *NRG1* hypomorphic mice was not reversed by clozapine at a dose of 1 mg/kg, although these studies need to be expanded.

16% Fewer Functional NMDA Receptors in the NRG1 *Mutant Mice*

We performed MK-801 binding studies of forebrain homogenates from *NRG1* hypomorphs generated by Gerlai et al. (2000) and control mice. The pK_D values were analyzed by ANOVA and did not reveal any differences between the wild-type and the mutant mice. Bmax values (pmoles/mg protein) in the mutants were found to differ significantly (one-sided P = .0068) from those in the wild-type mice, suggesting that there are 16% fewer functional NMDA receptors in the mutant animals overall (table 1). This is in keeping with reports suggesting a role for *NRG1* in regulation of NMDA subunit expression (Ozaki et al. 1997).

It is also of interest here that there appears to be reduction in the numbers of functional NMDA receptors

Table 1

[^{3}H] MK801 Binding

		Bmax VALUES (moles/mg protein)		
MOUSE	COUNT	Mean	SD	*P*
NRG1 knockout	16	1.23×10^{-12}	2.22×10^{-13}	6.8×10^{-3}
Wild type	18	1.43×10^{-12}	2.14×10^{-13}	

NOTE.—Concentrations of [^{3}H] MK801 in homogenates from forebrains of *NRG1* knockout and wild-type mice. One-sided *P* value is given.

in certain regions of brains from schizophrenic individuals (Ibrahim et al. 2000; Goff and Coyle 2001). We feel, however, that we have to caution that this does not necessarily mean that the principal pathogenic alteration in schizophrenia lies in the glutamate system.

Discussion

NRG1 *Provides a Way of Unifying a Large Body of Conflicting Evidence*

Through the work described above, we have identified the *NRG1* gene as a strong candidate for a gene playing a role in the pathogenesis of schizophrenia. We present three lines of evidence in support of this role for *NRG1*.

The first is genetic evidence, consisting of suggestive linkage of schizophrenia to chromosome 8p in Icelandic families, supported by suggestive linkage in other populations (Pulver et al. 1995; Kendler et al. 1996; Levinson et al. 1996; Blouin et al. 1998; Shaw et al. 1998; Kaufmann et al. 1998; Brzustowicz et al. 1999; Gurling et al. 2001). This evidence is further supported by highly significant association of overlapping haplotypes that contain only one known gene within the overlap, namely *NRG1*. The population attributed risk for the identified core haplotype is 16%, which is a substantial contribution to the public health burden. The weakness in the genetic evidence is that we have not yet found a clear pathogenic mutation, which may, however, be par for the course in the genetics of common diseases.

The second line of evidence is that mice hypomorphic for each of two mutations in *NRG1* and one mutation in a receptor for *NRG1* display behavior that overlaps, in part, with mouse models for schizophrenia, and this is reversed, in part, with clozapine in a *NRG1* mutant line.

The third line of evidence is that the number of NMDA receptors in the *NRG1* hypomorphs is reduced which is in keeping with observations made on brains from schizophrenia patients. Thus, these results argue that variants of the *NRG1* gene contribute to the pathogenesis of schizophrenia in some patients, probably through a decrease in *NRG1* signaling. The overlap in behavioral phenotype between the *NRG1* and *ErbB4* hypomorphic mice, and the lack of a similar behavioral phenotype in *ErbB2* or *ErbB3* mice (Gerlai et al. 2000), argues that the defect is primarily neuronal. Although each line of evidence is not conclusive, they constitute, when put together, a strong case for *NRG1* as a culprit in the pathogenesis of schizophrenia. Furthermore, the *NRG1* knockout mice provide a tool to explore this hypothesis further, on the basis of our understanding of the genetics of the disease.

The *NRG1* gene was identified as a schizophrenia gene by using a combination of a linkage and association approaches, based on microsatellite markers and then SNPs once microsatellite at-risk haplotypes were identified. Although SNP haplotypes are in general more stable and may capture the ancestral haplotype better than the overriding microsatellites, at-risk haplotypes in our study would not have been identified in a systematic manner without using the more cost-effective and informative microsatellite markers. In fact, our core at-risk haplotype is best represented by a combination of two stable microsatellites and one SNP.

Despite finding >1,200 SNPs in the *NRG1* gene and scoring 181 for association, we failed to find a clear functional polymorphism that captures the same degree of association as the schizophrenia at-risk core haplotype. SNPs screened were found within exons, promoters, splice sites, and regions of the gene most homologous between mouse and human. Our core at-risk haplotype represents a block of linkage disequilibrium that can be represented by just a few SNP and microsatellite markers. We continue to screen the large introns and flanking regions of the gene for associated variations, especially within the regions most conserved with the mouse.

NRG1 has not previously been considered in the context of schizophrenia. However, it is a fascinating candidate gene for the disease. A unique strength of the hypothesis that a defect in neuronal *NRG1* signaling underlies some cases of schizophrenia is that it brings together the disparate clinical and pathological features of this disease into a common pathway. *NRG1* isoforms (also called "ARIA," "GGF2," "NDF," "SMDF," and "heregulin," depending on the isoform and tissue in

which they were first identified) are a group of proteins that arise from alternative splicing of a single primary transcript (Fischbach and Rosen 1997; Wang et al. 2001). *NRG1* isoforms are expressed in many tissues, including the CNS, and these isoforms clearly have a developmental role, as indicated by knockout mice displaying severe developmental anomalies in the heart and the nervous system (Liu et al. 1998; Gerlai et al. 2000). An *NRG1* isoform originally discovered on the presynaptic membrane of the motor neuron (as ARIA) was found to be the factor inducing expression and localization of acetylcholine receptors (AchR) at the neuromuscular synapse. *NRG1* isoforms influence gliogenesis and neuronal migration during development of the brain, and, in the adult nervous system, *NRG1* appears to have a marked impact on the expression and activation of several neurotransmitter receptors, including NMDA glutamate receptors (Ozaki et al. 1997; Ibrahim et al. 2000), possibly Ca^{2+}-activated K^+ channels (Chu et al. 1995; Cameron et al. 2001), and it also facilitates neurotransmitter release from GABAergic interneurons.

The transmembrane forms of *NRG1* are present within synaptic vesicles, including those containing glutamate. After exocytosis, *NRG1* is in the presynaptic membrane, where the ectodomain of *NRG1* may be cleaved off. The ectodomain then migrates across the synaptic cleft and binds to and activates a member of the EGF-receptor family on the postsynaptic membrane. This has been shown to increase the expression of certain glutamate-receptor subunits. In addition, *ErbB4*, the predominant receptor for *NRG1* on CNS neurons, is colocalized with NMDA receptors in the postsynaptic density 95 complex (Garcia et al. 2000; Huang et al. 2000). In the CNS, the NMDA subunits, NR2A and NR2B, are heavily phosphorylated at tyrosine residues (Lau and Huganir 1995), and this posttranslational modification enhances receptor activity by altering the kinetic properties of the channel (Lau and Huganir 1995). Garcia et al. (2000) pointed out the possibility that the activity-dependent activation of *ErbB4* receptors by *NRG1* may regulate synaptic plasticity by recruiting tyrosine kinases that regulate NMDA receptor function. Thus, *NRG1* appears to signal for glutamate-receptor subunit expression, localization, and /or phosphorylation facilitating subsequent glutamate transmission. Therefore, the activity-dependent effects of *NRG1* and *ErbB4* on glutamatergic transmission efficiency may be one mechanism of synaptic plasticity. Abnormalities in synaptic plasticity may lead to the abnormalities in thought processes and cognition seen in schizophrenia that is out of proportion to the subtle decrease in glutamate receptors.

There are many pharmacologic and mouse mutant data that support the glutamate dysfunction hypothesis, and glutamate-receptor expression and binding may be decreased in schizophrenia patients (Huang et al. 2000). However, studies looking for variations in receptor subunits have not shown clear association to schizophrenia. Hypofunction of *NRG1* in schizophrenia, could explain, in part, the apparent deficiency in glutamate-receptor expression and binding described within in some parts of brains of schizophrenia patients (Huang et al. 2000). *NRG1* has additional roles in AchR expression. Abnormalities in PPI, the sensory gating of which may be mediated by nicotinic AchR in the hippocampus (Freedman et al. 1995; Holt et al. 1999) as well as the high rate of nicotine addiction in schizophrenic patients could be secondary to *NRG1* abnormalities. Thus, it is also possible that the *NRG1* abnormality causes schizophrenia through a mechanism in which the glutamate system plays a minor role.

Our behavioral data on the *NRG1* and *ErbB4* mouse mutants provide additional evidence for a role of *NRG1* in schizophrenia. We replicate the work done by Gerlai et al. (2000) on a different *NRG1* mutant and we show that both the *NRG1* and the *ErbB4* hypomorph mice are hyperactive, a phenotype that overlaps with behaviors induced by PCP in normal mice. Clozapine reduced the hyperactivity in the *NRG1* mice as it does in PCP-treated mice and mice with reduced numbers of NMDAR1 (NR1)–receptor subunits (Mohn et al. 1999). The clozapine reversal, therefore, further supports the possibility that the hyperactivity observed in the *NRG1* mice is related to schizophrenic phenotypes. In addition, the *NRG1* mice showed a defect in PPI, a psychomotor defect seen in some schizophrenic patients that can be evaluated in animals in a similar fashion.

Heterozygous *ErbB2* and *ErbB3* knockouts do not exhibit behavior abnormalities (Gerlai et al. 2000), but *ErbB4* is the predominant neuronal receptor for *NRG1* in the CNS (Steiner et al. 1999). It is not clear, at this point, how *NRG1* contributes to schizophrenia susceptibility, and it is likely that additional factors, such as environmental stress or variants of interacting genes, may be required to unmask the disease. Nevertheless, the availability of *NRG1* and *ErbB4* hypomorphic mice offers new opportunities for exploration of genetic and environmental interactions that may contribute to the pathogenesis of schizophrenia and for the development of novel therapies.

In summary, we have presented linkage, case-control haplotype-association, and TDT analyses that support the notion that *NRG1* contributes to schizophrenia. In addition, we present behavioral and pharmacological data on mouse mutants of *NRG1* and *ErbB4*, as well as glutamate-receptor–binding data supporting its proposed role in schizophrenia.

If *NRG1* is a schizophrenia susceptibility gene, its impact is unlikely to be limited to the Icelandic population,